Example of Proof Load Testing from Europe

Lantsoght, Eva; Hordijk, Dick; Koekkoek, Rutger; van der Veen, Cor

Publication date
2019

Document Version
Accepted author manuscript

Published in
Load Testing of Bridges

Citation (APA)
Lantsoght, E., Hordijk, D., Koekkoek, R., & van der Veen, C. (2019). Example of Proof Load Testing from Europe. In E. Lantsoght (Ed.), *Load Testing of Bridges: Proof Load Testing and the Future of Load Testing* (Vol. 13). CRC Press / Balkema - Taylor & Francis Group.

Chapter 15. Example of proof load testing from Europe

E.O.L. Lantsoght

Politécnico, Universidad San Francisco de Quito, Quito, Ecuador & Concrete Structures, Delft University of Technology, Delft, the Netherlands

D.A. Hordijk, R.T. Koekkoek, C. van der Veen

Concrete Structures, Delft University of Technology, Delft, the Netherlands

ABSTRACT: This chapter describes the proof load testing of viaduct Zijlweg at a position that is critical for bending moment and at a position that is critical for shear. The viaduct Zijlweg has cracking caused by alkali-silica reaction, and the effect of material degradation on the capacity is uncertain. Therefore, the assessment of this viaduct was carried out with a proof load test. This chapter details the preparation, execution, and evaluation of viaduct Zijlweg. The outcome of the proof load test is that the viaduct fulfils the code requirements, and that strengthening or posting is not required.

1 INTRODUCTION TO VIADUCT ZIJLWEG

1.1 **Existing bridges in the Netherlands**

Many of the existing bridges in The Netherlands were built in the decades of the European reconstruction after the Second World War. These structures are now approaching the end of the service life they were originally designed for. Additionally, the currently governing codes are prescribing larger live loads (representing the large traffic volumes and intensities as compared to the codes that were used at the time of design of these structures) and sometimes lower capacities (for example the shear capacity according to the Dutch NEN 6720:1995 (Code Committee 351001 1995) is higher than according to the NEN-EN 1992-1-1:2005 (CEN 2005)). As a result, the capacity of some existing bridges is subject of discussion (Walraven 2010). Other sources of uncertainty are the effect of material degradation or uncertainty about the available reinforcement when as-built plans are missing.

For the assessment of a bridge by calculation, different Levels of Approximation can be used. Each higher Level requires more computational time but also gives a value that is expected to be closer to the experimental (real) value, although still keeping a margin of safety into account (fib 2012). For reinforced concrete slab bridges in the Netherlands, the assessment on the first Level of Approximation is a hand calculation (Lantsoght et al. 2013, Vergoossen et al. 2013). If this calculation shows that the capacity of the bridge is sufficient, then it is not necessary to go to higher Levels of Approximation. If the calculation shows that the capacity is not sufficient, there is no indication that the real capacity is insufficient. A more refined calculation technique should then be used. For the assessment of bridges at Level of Approximation 2 a linear finite element calculation is used (Lantsoght et al. 2017a). If an even higher Level of Approximation is necessary, non-linear finite element calculations need to be made. Further Levels of Approximation include probabilistic analyses and coupling of non-linear finite element techniques with spatial variability of materials (Li et al. 2004) and the random distribution of loads.

Table 1: Considered safety levels governing in the Netherlands

Safety level	β	Ref period	γ_{DC}	γ_{DW}	γ_{LL}
Eurocode Ultimate Limit State	4.3	100 years	1.25	1.35	1.50
RBK Design	4.3	100 years	1.25	1.25	1.50
RBK Reconstruction	3.6	30 years	1.15	1.15	1.30
RBK Usage	3.3	30 years	1.15	1.15	1.25
RBK Disapproval	3.1	15 years	1.10	1.10	1.25
Eurocode Serviceability Limit State	1.5	50 years	1.00	1.00	1.00

If there are still uncertainties to determine if a given structure can carry the code-prescribed loads (for example, when the effect of concrete deterioration over time is unknown), then proof loading can be applied. In such a test, sufficient structural capacity of the bridge is proven by demonstrating that it can withstand a calculated proof load without causing irreversible (additional) damage. The proof loading can be applied with respect to different safety levels: disapproval level, reconstruction level, and the design level, as prescribed in the Dutch code NEN 8700:2011 (Normcommissie 351001 2011a). This Dutch code describes different safety levels, with associated different load factors, calibrated for different values of the reliability index (Steenbergen and Vrouwenvelder 2010). For existing bridges, and their associated consequence

class, these requirements, and the added "usage" level, are prescribed in the Guidelines for Assessment for Existing Bridges (Richtlijnen Bestaande Kunstwerken, RBK) (Rijkswaterstaat 2013). The load factors, reliability index β, and reference period ("ref period") are shown in Table 1, which shows the values used in NEN-EN 1990:2002 (CEN 2002), NEN 8700:2011 (Code Committee 351001 2011), and the RBK (Rijkswaterstaat 2013). The load factors that are listed in Table 1 are those used for the assessment of existing bridges: γ_{DC} for the self-weight, γ_{DC} for the superimposed dead load, and γ_{LL} for the live loads.

Proof load testing can be an interesting assessment method for the existing bridges in the Netherlands, and the technique can be used for different bridge types, owned by municipalities, provinces and the Ministry of Infrastructure and the Environment. When the technique of proof load testing will be standardized and streamlined, it can become a fast and economic method for the direct evaluation of existing bridges. To develop standardized procedures, a number of open research questions need to be answered. Therefore, a number of pilot proof load tests have been carried out in the Netherlands (Lantsoght et al. 2017e). The testing of viaduct Zijlweg (Lantsoght et al. 2017c), demonstrated in this chapter, formed part of this campaign of pilot proof load tests.

The difficulty in assessing viaduct Zijlweg is caused by the uncertainty on the capacity. The superstructure of viaduct Zijlweg is affected by alkali-silica reaction (ASR). The effect of ASR on the shear capacity of concrete elements is subject to discussion. Using a conservative approach to take into account the effect of ASR resulted in an insufficient assessment for the bridge. Therefore, viaduct Zijlweg is an excellent candidate for a pilot proof load test to investigate if the code requirements are fulfilled. The failure modes that were assessed through this load test were flexure and shear. Proof load testing for shear is a novel application, as this brittle failure mechanism requires additional preprations.

The viaduct Zijlweg is representative of the viaducts affected by ASR in the Netherlands. In total, between 40 and 50 structures (bridges, tunnels, and locks) have material degradation caused by ASR (Nijland and Siemes 2002). The aggregates that contain reactive silica leading to ASR are porous chert, chalcedony and impure sandstones that often react as porous chert. Viaduct Zijlweg forms part of a series of bridges in and over the highway A59, built during the 1960s and 1970s, which are all affected by ASR. A number of the viaducts with ASR-damage are posted, strengthened, and/or monitored (Borsje et al. 2002). For viaduct Zijlweg, monitoring is used. Maintenance activities focus on preventing the ingress of moisture so that the swelling of the ASR-gel is stopped. Monitoring activities focus on the moisture content and deformations and aim at assessing the effectiveness of the rehabilitation strategies.

1.2 **Viaduct Zijlweg**

1.2.1 *General information and history*

The Ministry of Infrastructure and the Environment commissioned the TU Delft to perform a proof load test on the viaduct Zijlweg (Fig. 1) over the highway A59 in the Zijlweg between Waspik and Raamsdonksveer, see Fig. 2. Viaduct Zijlweg is a reinforced concrete slab bridge with 4 spans. The spans are supported by concrete piers at the mid supports and by an abutment at the end supports. The forces from the deck are transferred via elastomeric bearing pads to the piers and abutments. It was built in 1965 for the province of Noord Brabant with a design life of 80 years.

Viaduct Zijlweg is one of a series of viaducts in and over the A59 highway with Alkali-Silica Reaction (ASR). This viaduct was field tested as the influence of ASR on the capacity was uncertain and complicated the analytical assessment. In 1997, ASR was detected in the viaduct Zijlweg (Projectteam RWS/TNO Bouw 1997b). Material testing at that time led to the observation that the uniaxial tensile strength is very small, which, in addition to the large number of cracks observed, resulted in concerns with regard to the shear capacity. As typical for reinforced concrete slab bridges, the structure does not contain shear reinforcement. Moreover, the bridge was designed for class 30 from VOSB 1963 (Nederlands Normalisatie Instituut 1963) but is currently in use as class 45.

Fig. 1 : Viaduct Zijlweg in the highway A59 in the province Noord Brabant.

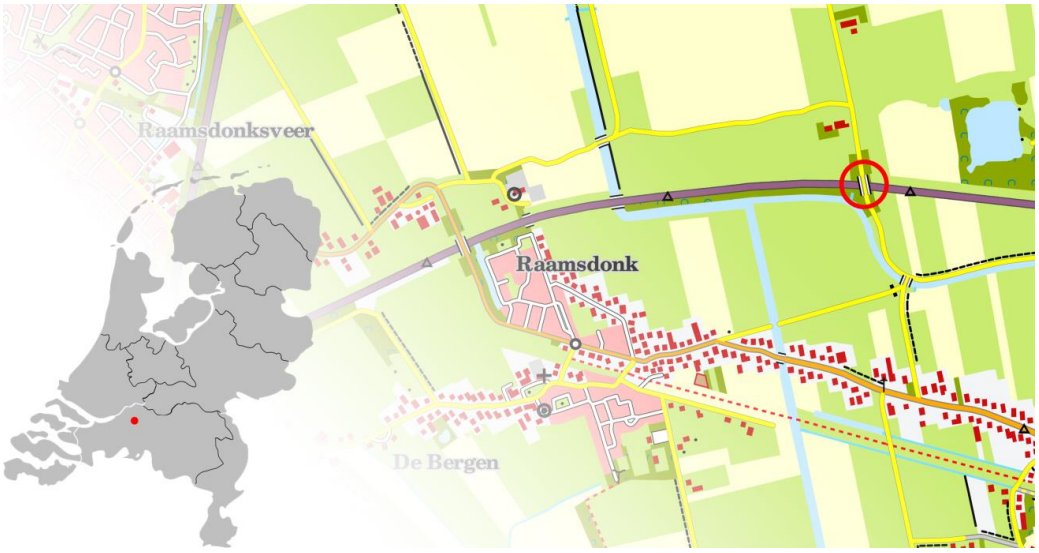

Fig. 2: Location of viaduct Zijlweg

In 2002, the most recent renovation of viaduct Zijlweg was done (Rijkswaterstaat 2002). At that time, the concrete of the main superstructure was repaired with cement-bound polymer-modified mortar, the damage caused by ASR was inspected, the concrete at the support was re-paired, the asphalt layer was inspected and replaced, the joint at the end support was replaced and inspected, maintenance was given to the handrail, the concrete of the sidewalk was repaired, and all other concrete elements were inspected. According to the maintenance and management plan of viaduct Zijlweg, the main superstructure and supports should be inspected every five years. The joints are to be given maintenance every 20 years, and the handrail every 12 years. The waterproofing layer of the concrete should be replaced every 12 years.

1.2.2 *Material properties*

The concrete compressive strength is determined based on cores drilled from the viaduct (Witteveen+Bos 2014). The average cube concrete compressive strength was found to be $f_{c,cube,m}$ = 44.4 MPa (6.4 ksi) and the characteristic concrete cylinder compressive strength is f_{ck} = 24.5 MPa (3.6 ksi). Experimental results about the properties of the reinforcement steel are not avail-able. The symbols on the reinforcement drawings indicate that plain bars QR22 or QR24 (not specified which steel grade) were used. For QR22, the characteristic yield strength is f_{yk} = 220 MPa (32 ksi), and for QR24 f_{yk} = 240 MPa (35 ksi).

1.2.3 *Structural system and description of tested span*

Viaduct Zijlweg crosses the highway under an angle of 75.6°. The length of the end spans is 10.32 m (34 ft) and the length of the central spans is 14.71 m (49 ft), as can be seen in Fig. 3.

Fig. 4 shows the numbering of the spans and the location of the tested span. Span 4 chosen because it is not directly above the highway A59, so that closing of the highway is not necessary during the proof load test. The width of the viaduct is 6.60 m (22 ft) and the width of the carriageway is 4.00 m (13 ft). Only a single lane is available, and vehicles need to take turns in entering the viaduct. A sidewalk of 1.3 m (4 ft) wide is located on both sides, see Fig. 5.

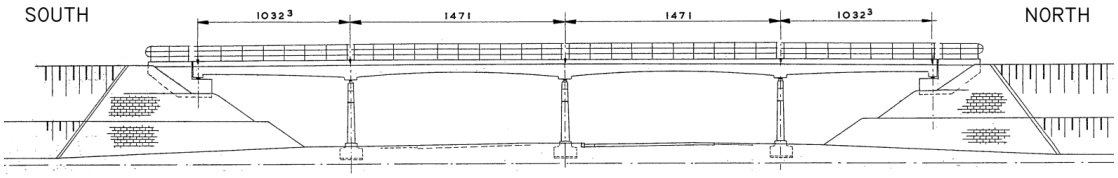

Fig. 3: Structural system of the viaduct in the Zijlweg. Units: [cm]. Conversion: 1 cm = 0.4 in

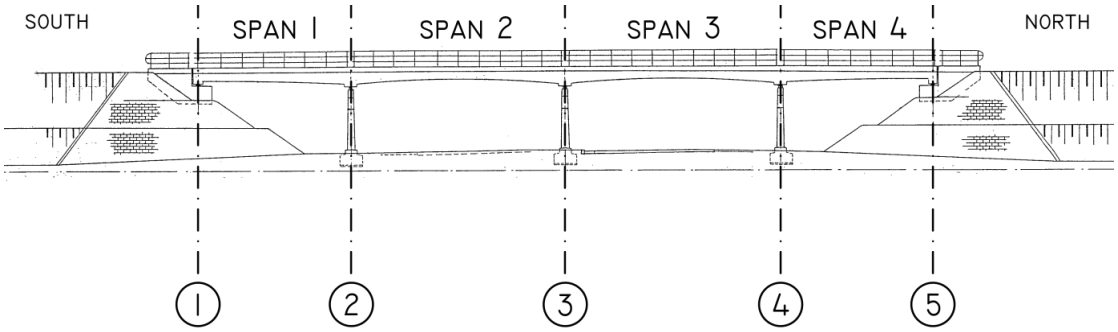

Fig. 4: Numbering of the spans and supports.

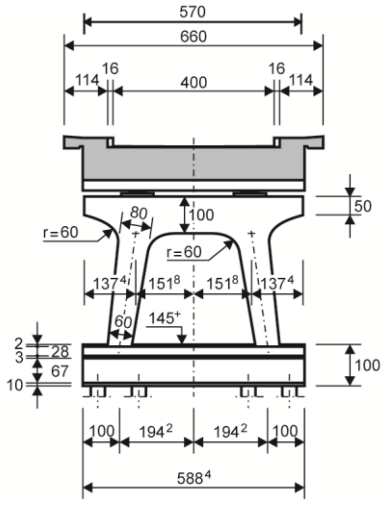

Fig. 5 Sketch of cross-section. Units: [cm]. Conversion: 1 cm = 0.4 in.

Span 4 has a variable thickness. The thickness is 550 mm (22 in) at support 5 and increases to 850 mm (33 in) at support 4. The thickness varies parabolically with a radius of curvature r = 150 m (495 ft), see Fig. 6. The layout of the reinforcement in span 4 is shown in Fig. 7.

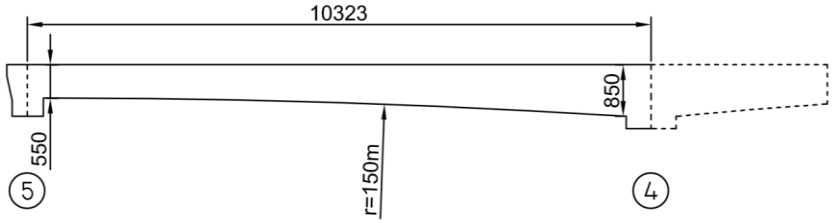

Fig. 6 Longitudinal view of span 4.

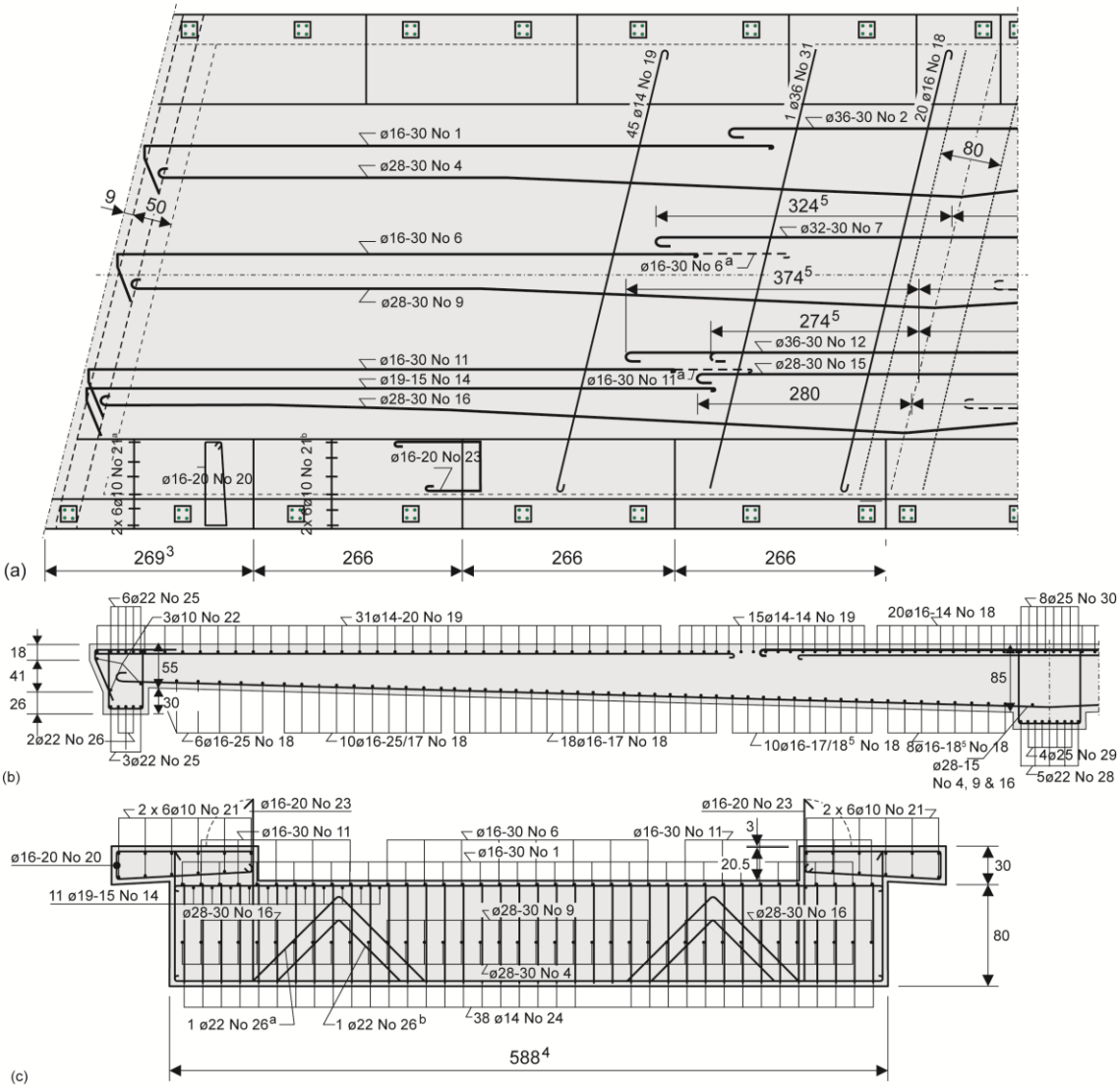

Fig. 7: Reinforcement in span 4: (a) top view; (b) side view; (c) cross-beam. Units: bar diameters in [mm] and other dimensions in [cm]. Conversion: 1 mm = 0.04 in, 1 cm = 0.4 in. Reprinted with permission from (Lantsoght et al. 2017c).

2 PREPARATION OF PROOF LOAD TEST

2.1 **Preliminary assessment**

In the Netherlands, an assessment is carried out based on the Unity Check, which is the ratio of the factored load effect to the factored capacity. If the Unity Check is larger than 1, the cross-section is found not to fulfil the code requirements. For span 4 of viaduct Zijlweg, an initial assessment resulted in a Unity Check of 5.4 at the end support for shear. Therefore, in accordance to the approach with different levels of assessment (Lantsoght et al. 2017b), a refined calculation was carried out. The tensile strength was determined based on 51 specimens in uniaxial tension and 10 specimens in splitting tension, and finite element calculations were used to determine the acting sectional shear. The highest Unity Check with this refinement was UC = 1.31 at support 4 (see Fig. 4) (Projectteam RWS/TNO Bouw 1997a). For this purpose, the viaduct Zijlweg was considered a good candidate for a proof load test.

2.2 **Inspection**

The inspection that was planned for 2007, was carried out on April 18th 2008. A visual inspection was used to fine-tune the plan for future repair and inspections. The analysis of the inspection was based on risk, see

Table 2. Based on the calculated risk, it is decided whether a given risk is acceptable or not. For unacceptable risks, actions for management and maintenance are proposed. In the conclusions of the report, the risk associated with the insufficient capacity of the superstructure was emphasized. The viaduct was considered to be in moderate conditions. Maintenance actions were proposed for 2019 (replacement of asphalt upper layer, repair of deck, sidewalk, and support, cleaning of bearings, and conservation of steel handrails) and 2025 (replacement of full asphalt layer). From the analysis of the ASR measurements, it was concluded that the expansion in the longitudinal direction was reaching its maximum value.

Table 2: Overview risks and recommendations from inspection 2008.

Bridge part	Problem	Explanation	Recommendation
Entire structure	Assumptions of design do not correspond with current use	Increase of traffic intensity	- Try to find out traffic load class - Assessment through recalculation of structural capacity
	Assumptions of design do not correspond with current use	Change in usage	No action required
	Design errors	Design errors	No action required
Concrete general	Cracking caused by ASR	Swelling causes disintegration of concrete, resulting in reduced capacity	- Monitoring is in place - No further actions required
	Cracking caused by shrinkage	Shrinkage and thermal stresses lead to cracks with a large width, resulting in durability issues	- Further research to determine which part of cracking is caused by ASR and which part by shrinkage
Main load carrying structure: deck and supports	Spalled parts caused by impact, loose filling of locations of drilled cores, failed repair	Spalled parts can fall down later. Loss of cover results in corrosion of steel and further spalling of concrete	- Repair of impact damage - Add to regular maintenance
	Spalling of concrete caused by	Spalled parts can fall down later. Loss of cover results in corro-	- Regular maintenance

	corrosion	sion of steel and further spalling of concrete	
Handrail	Possible accidents from large openings in handrail	Handrail consists of horizontal parts that children can use to climb and fall through	- Attention owner of structure
Supports	Elastomeric bearings show cracking and are in their furthest position	Support is not able to carry the loads to the foundations in a correct manner	- Possibly caused by ASR - Same actions as for ASR
Sidewalk	Spalling, loose filling of cores, shrinkage cracks, poor compaction of concrete	Increased deterioration from deicing salts, caused by poor maintenance of the concrete surface. Possibility for future corrosion of reinforcement.	- Add to regular maintenance
Joint (steel + rubber)	Steel of joint is rusted and rubber has been damaged	Possible damage from chlorides in structure and damage of traffic by loosening of finger joint. Damage attributed to traffic loads. Water tightness and safety are compromised.	- Add to regular maintenance

A visual inspection was carried out during the preparation stage of the proof load test. Fig. 8 shows the deterioration of the top deck, present in the pedestrian sidewalk. Fig. 9 shows an impression of the bottom of the deck. The typical cracking pattern of ASR (map cracking) is not clearly visible from the distance at which the inspection was carried out. Closer observations on scaffolding right before the execution of the proof load test allowed for the drawing of the full crack map, see Fig. 10. Fig. 11 shows the small distance remaining in the joint, resulting from the expansion in the longitudinal direction.

Fig. 8: Top deck

Fig. 9 Bottom of deck.

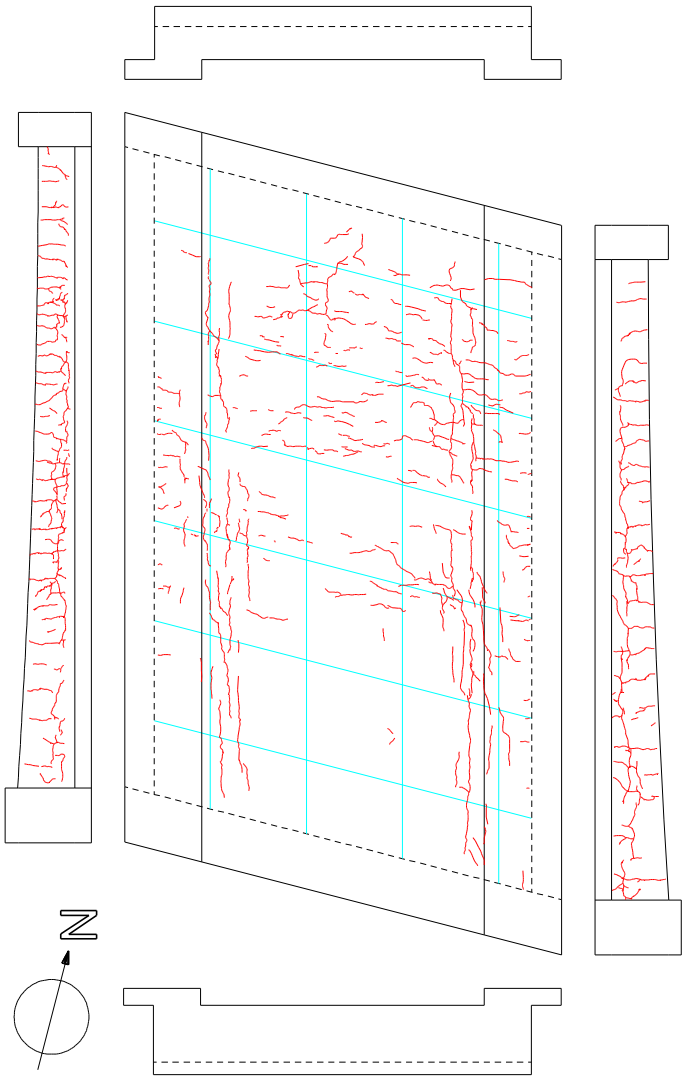

Fig. 10 Observed cracking pattern, showing cracking on bottom face of slab and side faces. From (Lantsoght 2017), reprinted with permission.

Fig. 11 Expansion joint at the South side of viaduct Zijlweg.

2.3 **Effect of Alkali-Silica Reaction**

2.3.1 *Effect of Alkali-Silica Reaction on capacity*

Alkali-Silica Reaction (ASR) is the reaction between the reactive (glasslike) silica that is present in aggregates from some sources and alkali that is present in cement paste (Neville 2012). The result of this reaction is a gel of calcium silicate hydrate. Upon contact with water, this gel will expand, and this expansion causes stresses in the concrete. If these stresses exceed the tensile strength of the concrete, cracking occurs. The expansion and resulting internal stresses in the concrete are influenced by the geometry and structure. For example, the existence of reinforcement limits the ASR expansion in the direction of the bars. In the vertical direction where no reinforcement is present, the expansion will not be limited. As a result, cracking occurs parallel to the reinforcement.

The effect of ASR on the concrete strength is typically expressed as a reduction on the strength as a function of the amount of free expansion of the concrete (Siemes et al. 2002). In the literature, the reduction of the tensile strength due to ASR is reported to vary between 5% (Ahmed et al. 1999) and 82% (Siemes et al. 2002). Research (Siemes et al. 2002) showed that the uniaxial tensile strength is lower than the expected value based on the compressive strength determined from testing cores or derived from the splitting tensile strength. The ratio of uniaxial tensile strength to the splitting tensile strength tested on core samples varied between 0.18 and 0.77; with an average of 0.5 for an expansion of 0.5‰ to 1.0‰ (Siemes et al. 2002). These high values, however, result from uniaxial tension tests on cracked specimens, in which the stress flow is disrupted. Moreover, the existing cracking reduces the area. Therefore, the use of uniaxial tension test on specimens affected by ASR may not be advisable. While generally the tensile

strength of concrete is neglected in design calculations, it plays an important role in the bond and anchorage strength, the shear and punching strength of members without shear reinforcement, the resistance against splitting caused by dowel action, and the load transfer in plain concrete elements such as footings. Low uniaxial tensile strengths are not unique for structures with ASR damage, but have also been found in relatively old structures where no ASR is present (Siemes et al. 2002, Yang et al. 2010).

Since bending moment capacity is governed by crushing of the concrete (failure of concrete in compression), ASR is expected not to have an influence on the bending moment capacity. Experiments showed that no clear conclusions on the influence of ASR on the concrete compressive strength can be drawn (Giaccio et al. 2008). One series of experiments (Talley 2009) confirms that no reduction in the moment capacity occurs, unless a high expansion has taken place, in which case 25% reduction of the bending moment capacity was found. Another comparison between a reinforced concrete member with and without ASR damage on a small scale (Haddad et al. 2008) found that the flexural capacity of a specimen with ASR damage was lower than the specimen without damage. The reduction of the capacity due to ASR-damage was 11%. The serviceable load and flexural stiffness of the ASR-damaged element were increased. The precompression of the concrete on the tension side delayed the crack initiation in the ASR beam as compared to the control beam. Once the precompression was offset at the tension side, during loading, the shift of the neutral axis toward the compression zone would be faster in the ASR-damaged specimens as compared to that of the control specimens because of the lower splitting strength of the damaged concrete and the "prestress" in the compression zone. The flexural failure of the ASR-affected beams was more abrupt than that of the unaffected beams.

Since shear failure is related to the tensile capacity of the concrete, ASR is expected to reduce the shear capacity. On the other hand, the precompression in the direction of the reinforcement may reduce or even revert this reduction as it increases the aggregate interlock capacity of the beams when the crack width is decreased. Measurements by (Ahmed et al. 1998) showed that the introduction of compression reinforcement reduced the expansion from ASR. ASR caused an irreversible upward deflection of the beam that was largely proportional to the amount of expansion measured in the beams. In fatigue testing a larger fatigue life was found for the specimens affected by ASR. In an overview of the literature, Schmidt et al. found that sometimes experiments indicate that ASR cracks lead to a reduction of the shear capacity and sometimes do not lead to a reduction of the shear capacity (Schmidt et al. 2014). In an exceptional case, an increase of 78% of the shear capacity was observed. When carrying out shear tests on bridge deck slabs, the measured capacity was found to exceed the calculated capacity for most of the cases (depending on the assumptions for the cross-sectional height and depending on the position

along the bridge). More than anything, the test results open the question whether the compressive strength from drilled out cylinders provides the right basis for evaluation of the shear capacity (Schmidt et al. 2014). Most experiments on the effect of ASR on shear have been carried out on beams of small size that were cast in the laboratory. Experiments on beams sawn from two 35-year-old viaducts with ASR damage are available in the literature, see Fig. 12 (den Uijl and Kaptijn 2002). Material testing on the bridges from which the beams were sawn showed a small uniaxial tensile strength. Comparing the experimental test results to the predicted value from Rafla's equation (Rafla 1971) showed that for the beams that failed in shear (from the second viaduct), a tested to predicted ratio of 0.77 (with a coefficient of variation of 7.5%) was found. In the conclusions, the recommendation was given to reduce the shear capacity of reinforced concrete members affected by ASR by 25%. This recommendation is used in the Netherlands to determine the shear capacity of ASR-affected members. Note that this recommendations is based on a comparison to a formula derived from a shear database, and that this formula possibly does not correctly take the size effect into account. A last series in which the effect of low direct tensile strength was studied on old and new concrete showed a ratio of uniaxial tensile strength to splitting tensile strength $f_{ct}/f_{ct,spl}$ of 47% for old concrete taken from an existing viaduct and 70% for beams cast in the lab (Yang et al. 2010). Upon testing, no clear differences between the old and new beams with regard to the failure mode, cracking load and ultimate load could be observed. This result seems to confirm that the low uniaxial tensile strength of ASR-affected members does not automatically imply small shear capacities.

Fig. 12: Testing of beams with ASR-damage in the Stevin Laboratory (den Uijl and Kaptijn 2002). Photograph by J. A. Den Uijl, used with permission.

2.3.2 *Load testing of ASR-affected viaducts*

In the literature, reference to a number of load tests on ASR-affected viaducts are available. The first example is the proof loading of a bridge in the Hanshin expressway in Japan. Testing to 80% of the design load showed sufficient capacity of the bridge. The difference in deflection between the elements with damaged and undamaged concrete was less than 0.2 mm (0.008 in). A second example are the bridges in the A26 highway in France, several of which are suffering from ASR-damage. Diagnostic testing of new bridges is standard practice in France, so that baseline information is available (Talley 2009). Load testing can thus give a comparison to the initial state of the bridge upon completion of the construction. It was found in a reference case that the reduction in stiffness of the viaduct was less than 10%. Repair after the load test consisted of applying a coating to prevent further moisture ingress. A third example includes testing to 85% of the design capacity on a double deck road structure in South Africa, which led to the conclusion that this structure was adequate (Talley 2009). A final example relates to ASR-affected bridges in Denmark (Schmidt et al. 2014), tested to evaluate their performance in shear. It was found that the compressive strength and splitting tensile strength were reduced significantly compared to the design strengths while no reduction of the shear capacity was found.

2.3.3 *Monitoring results*

Since 2003, monitoring of the viaduct Zijlweg for ASR is in place (Koenders Instruments 2015). An update of the equipment was provided in 2007. Sensors are applied in spans 1 and 4, measuring temperature, thickness of the deck, moisture in the concrete, and the longitudinal expansion of the deck. The data analysis of 2008 (Rijkswaterstaat 2008) concluded that shrinkage was occurring over the depth of the cross-section, expansion was occurring over the longitudinal direction, and the moisture content is increasing.

Prior to the proof load test, the available data are analysed. The analysis uses the environmental data obtained from the KNMI (Royal Dutch meteorological institute) at a weather station 14 km (8.7 mi) south of the proof loading location (Royal Dutch Meteorological Institute 2017). There is a clear correlation visible between the fluctuations of the temperature over the year and the thickness, joint size or moisture content, see Fig. 13. Since the beginning of the year 2009 a clear increase in thickness is visible. Fig. 13a shows the relation between the average thickness of the cross-section and the ambient temperature. The joint size (Fig. 13b) is inversely correlated to the temperature. This effect is due to the expansion of the bridge at higher temperatures, which results in a smaller joint size. The joint size gradually decreases over time, which means that the bridge is expanding longitudinally. Considering the moisture content in Fig. 13c a clear

fluctuation of the moisture content with an average of 10% can be seen. From Fig. 13d it can be concluded that there is a good correlation between the ambient and deck temperature.

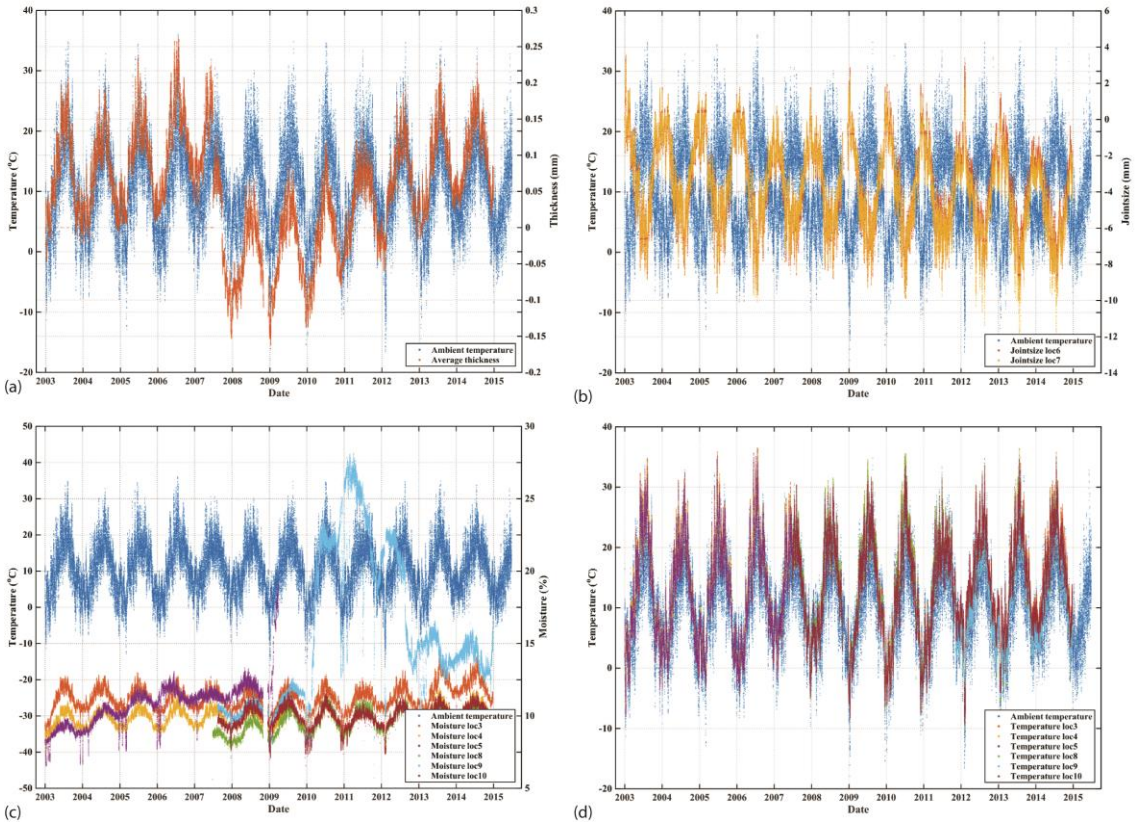

Fig. 13: Data of ASR-sensors: (a) relation between ambient temperature and average deck thickness; (b) relation between ambient temperature and joint size; (c) relation between ambient temperature and moisture in the deck; (d) relation between ambient temperature and measured temperature at the deck.

2.4 **Determination of target proof load and position**

2.4.1 *Finite element model*

The target proof load was determined based on a linear finite element model, developed with TNO Diana (TNO DIANA 2012). The slab was modelled with a uniform thickness, and the larger depth of the sidewalk was not taken into account. Eight-node quadrilateral isoparametric flat shell elements were used. The final mesh contains 106 elements in the length direction and 12 elements in width direction. Each crossbeam of the viaduct is supported at two locations.

The permanent loads used in the model include the self-weight of the structure and the super-imposed dead load. A density of 2500 kg/m^3 (150 pcf) is used for the concrete. The equivalent load of the elements that are not modelled is added. These elements are the sidewalks, the wear-

ing surface, and the asphalt layer. For the wearing surface a load of 1.15 kN/m^2 (24 psf) is used. The width in the model is 5.7 m (18.7 ft), which is smaller than the full width of 6.6 m (21.7 ft) shown in Fig. 5, so that a distributed load to represent the additional width is added. For the asphalt layer, a load of 2.5 kN/m^2 (52 psf) is applied, which corresponds to a layer of 100 mm (4 in) thickness.

The variable loads used in the model are in accordance with live load model 1 from EN 1991-2:2003 (CEN 2003), which combines a distributed lane load with a design tandem per lane. The notional lane width is 3 m (10 ft). The distributed lane load is 9 kN/m^2 (188 psf). To find the largest load effects in span 4, the lane load is applied in spans 2 and 4, whereas no distributed lane load is applied in spans 1 and 3. The remaining part of the actual lane of the viaduct is loaded with a load of 2.5 kN/m^2 (52 psf). On the sidewalks, a pedestrian load of 5 kN/m^2 (104 psf) is used. The design tandem consists of two axles of 300 kN (67 kip) spaced 1.2 m (4 ft) apart. The wheel print of the tandem is 400 mm × 400 mm (15.7 in × 15.7 in). For the considered model using shell elements, only the mid-depth of the cross-section is modelled. It is assumed that the concentrated wheel loads are distributed under 45^o to the mid-depth, resulting in a surface of 950 mm × 950 mm (37.4 in × 37.4 in). In the model, the concentrated loads are applied as a distributed load of 155 kN/m^2 (3.3 ksf) on a surface of 2 elements by 2 elements. The tandem is centred in the notional lane. The Dutch National Annex NEN-EN 1991-2/NA:2011 (Normcommissie 351001 2011b) permits the use of reduction factors for bridges and viaducts subjected to less than 250,000 vehicles per year. These factors are 0.97 for the lane load, and design tandem, and 0.90 for the remaining area of the lane. As the factor only relates to the number of vehicles, it does not affect the modelled pedestrian traffic.

The load factors that are used for the load combination are as described by the Dutch guidelines for the assessment of bridges ("RBK" (Rijkswaterstaat 2013)), see Table 1. Table 3 gives an overview of the safety factors that are used for the load combinations at different safety levels in combination with proof load testing. These load combinations are all altered for γ_{DC} with regard to the prescribed load factors in the code. For all cases, γ_{DC} = 1.10. This value is used since the self-weight of an existing structures is not a random variable anymore, but can be considered as a deterministic value. Only the model factor remains (Walraven 2012).

Once the loads are defined, the governing sectional moment and shear have to be found. For this purpose, the position of the design truck is changed to a flexure-critical and shear-critical position, respectively. To find the flexure-critical position, the truck is moved along span 4 until the position is found that results in the largest sectional moment. To find the shear-critical position, the truck is placed at 2.5d_l with d_l the effective depth to the longitudinal reinforcement

(Lantsoght et al. 2013). Note that this distance was developed as the critical distance for straight slab bridges, and that no experimental evidence is available about its validity for skewed bridges. For a skewed viaduct, the critical position occurs in the obtuse corner (Cope 1985). The peak shear stress is then distributed in the transverse direction over $4d_l$ to find the representative sectional shear stress (Lantsoght et al. 2017a). The flexure-critical position in span 4 is at 3382 mm (11 ft) from the face of the support, see Fig. 14. The shear-critical position in span 4 is at 1208 mm (4 ft) from the face of the support. The contributions of the different loads to the total sectional shear at the cross-section at $0.5d_l$ from the support is shown in Fig. 15. These contributions are then summed and averaged over $4d_l$ to find the governing sectional shear that should equal the sectional shear caused by the load combination with the proof load tandem.

Table 3: Load factors in combination with proof load testing at different load levels.

	γ_{DC}	γ_{DW}	γ_{LL}
ULS	1.10	1.35	1.50
RBK Design	1.10	1.25	1.50
RBK Renovation	1.10	1.15	1.30
RBK Usage	1.10	1.15	1.25
RBK Disapproval	1.10	1.10	1.25
SLS	1.00	1.00	1.00

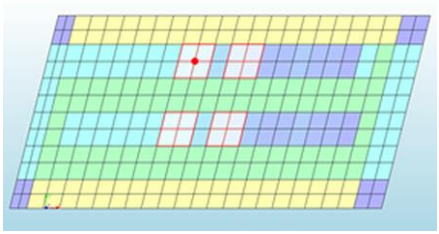

Fig. 14 Position of wheel loads for flexure-critical case.

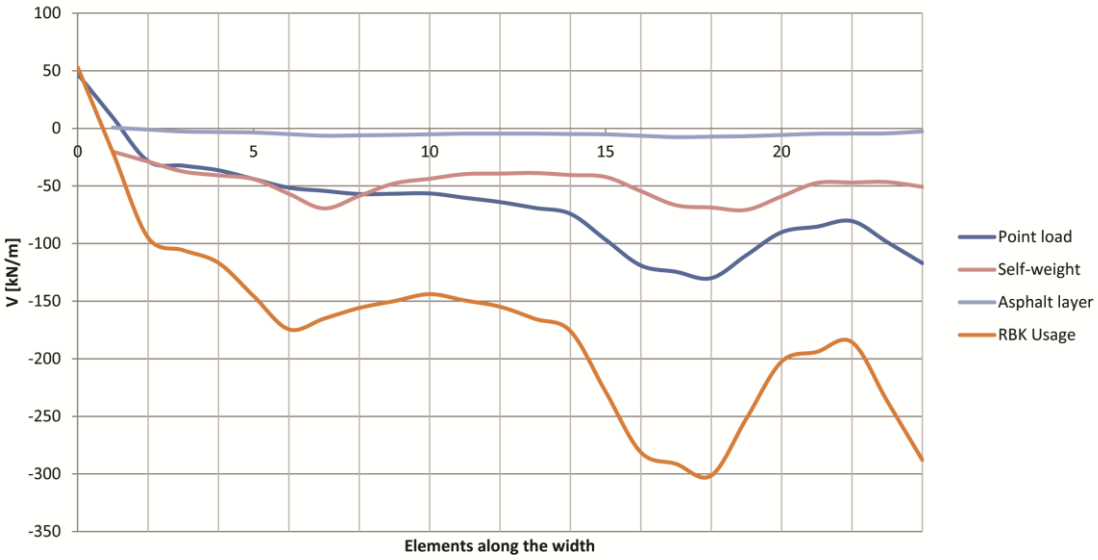

Fig. 15: Sectional shear over width of slab. The x-axis shows the numbering of the elements in the finite element model. Conversion: 1 kN/m = 0.07 kip/ft.

Table 4: Results of applied loads in linear finite element model. Conversion: 1 kNm/m = 0.225 kipft/ft.

Load	Moment [kNm/m]	γ	γ × Moment [kNm/m]	α	M_{Ed} [kNm/m]
Self-weight	-84.1	1.10	-92.5	1.00	-92.5
Asphalt layer	-7.7	1.15	-8.8	1.00	-8.8
UDL Notional Lane	-56.7	1.25	-70.9	0.97	-68.7
UDL Remaining Area	-4.7	1.25	-5.9	0.90	-5.3
Eurocode tandem	-184	1.25	-229	0.97	-222
Pedestrian traffic sidewalk	-12.1	1.25	-15.1	1.00	-15.1
		Total:	-423		-413

An example of the results using the RBK (Rijkswaterstaat 2013) Usage load level is shown in Table 4. First, the bending moment caused by the different loads is calculated separately. The resulting moment for the Eurocode tandem is obtained at the flexure-critical position. Then, each load is multiplied by the load factor γ, and subsequently by the factor that takes the reduced traffic into account, α. Then, to find the bending moment caused by the code-prescribed

loads at the RBK Usage level, all contributions are summed, and a bending moment M_{Ed} = 413 kNm/m (93 kipft/ft) is found.

2.4.2 *Resulting target proof load*

For the proof load, the wheel print of Rijkswaterstaat is used, which has a size of 230 mm × 300 mm (9 in × 12 in). For the application in the finite element model, which uses shell elements, vertical load distribution to the middle of the cross-section is used. The wheel print in the finite element model is then 780 mm × 850 mm (31 in × 33 in).

Table 5: Results for required proof loads P_{tot} at different safety levels for the flexure-critical and shear-critical positions. Conversion: 1 kN = 0.225 kip, 1 metric ton = 1.1 short tons.

	Bending moment		Shear	
Safety level	P_{tot} (kN)	P_{tot} (metric ton)	P_{tot} (kN)	P_{tot} (metric ton)
EC	1259	128	1228	125
RBK Design	1257	128	1228	125
RBK Reconstruction	1091	111	1066	109
RBK Usage	1050	107	1027	105
RBK Disapproval	1049	107	1025	104
SLS	815	83	791	81

The position of the design truck is moved along span 4 in order to find the position at which the largest bending moment results – the flexure-critical position. Then, the live loads from the Eurocode are removed, and the permanent loads remain in place. Subsequently, the proof load tandem is placed at the flexure-critical position. Then, the magnitude of the proof load is determined so that the maximum sectional moment caused by the factored permanent loads and the proof load tandem becomes the same as the maximum sectional moment resulting from the factored Eurocode live loads and permanent loads. Since this comparison is based on factored loads, the load factors associated with the considered safety level (see Table 1 for the prescribed load factors and Table 3 for the application to proof load testing) govern. A flowchart summarizing this procedure is given in Fig. 16.

The same procedure is used for the shear-critical position, for which the critical position is taken at $2.5d_l$ and the peak shear stress is distributed in the transverse direction over $4d_l$. A summary of the results for the flexure-critical and shear-critical position is listed in Table 5.

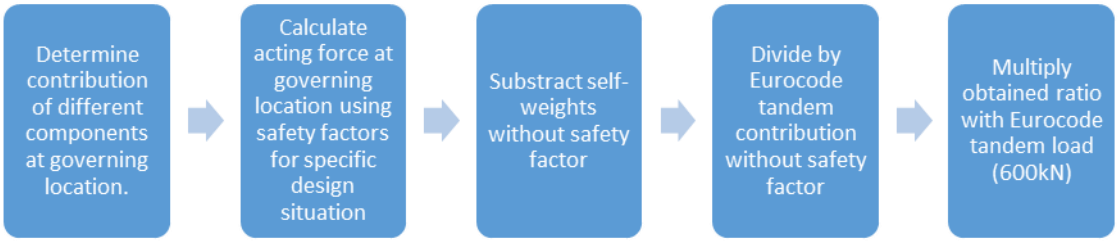

Fig. 16: Flowchart for determination of required proof loads.

2.5 **Expected capacity and behavior**

Part of the preparation of a proof load test includes estimating the capacity of the viaduct, and relating the expected capacity to the load that can be applied to the bridge. The values of the expected maximum load at a certain position of the proof load tandem help to know when meticulous attention must be paid to the measurements and stop criteria. For the preparation of the proof load test, all failure modes need to be considered. For this purpose, the capacity of the viaduct has to be determined for flexure, shear, and punching.

Table 6: Bending moment M and curvature κ at cracking, yielding and ultimate. Conversion: 1 kNm/m = 0.225 kipft/ft and 1/mm = 25.4 1/in.

	QR22			QR24		
	Cracking	Yielding	Ultimate	Cracking	Yielding	Ultimate
M (kNm/m)	204	383	413	204	415	459
κ (10^{-6} 1/mm)	0.372	2.69	68.2	0.372	2.91	61.2

First, the bending moment capacity is determined and the expected moment-curvature diagram is developed. The results for the cracking, yielding and ultimate moment are given in Table 6 for the cross-section with the maximum sagging moment, and the results of the unity checks based on a unit meter of width are given in Table 7 for both QR 22 and QR 24 steel. In Table 7, M_{Ed} is the sectional moment caused by the load combination prescribed by the code,

and $M_{Rd,c}$ is the capacity as prescribed by the code. These results show that a priori the viaduct could not be deemed satisfactory for bending moment capacity at all safety levels (as defined in Table 1), since for the Design safety level, the Unity Check is larger than 1.

Table 7: Bending moment capacity $M_{Rd,c}$, sectional moment M_{Ed} and resulting unity checks UC. Conversion: 1 kNm/m = 0.225 kipft/ft.

	QR 22		QR 24	
	RBK Usage	RBK Design	RBK Usage	RBK Design
M_{Ed} (kNm/m)	413	476	413	476
$M_{Rd,c}$ (kNm/m)	413	413	459	459
UC	1.00	1.15	0.90	1.04

Two levels of approximation (Lantsoght et al. 2017b) were followed to check the shear capacity at the shear-critical cross-section: Level of Approximation I (Quick Scan (Vergoossen et al. 2013)) and a Level of Approximation II (linear finite element analysis (Lantsoght et al. 2017a)). The shear capacity of concrete affected by ASR is assumed to be reduced by 25% (den Uijl and Kaptijn 2002). In the Level of Approximation I, the Quick Scan sheet is used in a load combination consisting of the self-weight, superimposed dead load, and proof load tandem. To find the maximum load that can be applied, the proof load is increased until a Unity Check of 1 is found. The results are given in Table 8 for the RBK (Rijkswaterstaat 2013) Usage and Design safety levels. The column with "Mean" is the resulting maximum load when all load and resistance factors are taken as equal to one and average instead of material properties are used. The value of P_{max} is the total maximum load for which a Unity Check UC = 1 is found for the considered safety level. The value of $P_{max,ASR}$ takes the capacity of the ASR-affected cross-section as 75% of an undamaged cross-section. The row with "UC" gives the resulting Unity Check for the cross-section, taking into account the effect of ASR-damage, at the considered safety level and using the code-prescribed loads. These Unity Checks are calculated for the values of P_{tot} from Table 5. These calculations considered the obtuse corner, as in the obtuse corner a larger concentration of shear stresses occurs (Cope 1985). For the reinforcement, QR 24 is assumed, since the yield strength of the steel is inversely proportional to the lower bound of the shear capacity v_{min} (Walraven 2013). A lower steel quality would thus result in a higher value of v_{min}, so that it is conservative to assume QR 24 for the determination of the shear capacity.

Table 8: Results for shear capacity at obtuse corner: maximum load to have a Unity check = 1 based on the Quick Scan spreadsheet, and Unity Check for code-prescribed loads. Conversion: 1 kN = 0.225 kip, 1 metric ton = 1.1 short tons.

	Usage	Design	Mean
P_{max} (kN)	1644	1136	4360
$P_{max,ASR}$ (kN)	1233	1002	3270
UC	0.833	1.225	--

Next, the Unity Check for shear was determined at a Level of Assessment II. The peak sectional shear force v_{Ed} resulting from the factored loads is distributed over 4d and then compared to the shear capacity $v_{Rd,c}$ and v_{min} as used in Level of Assessment I. The results for the Unity Check are given in Table 9, from which it can be seen that, the calculations indicate that the shear-critical cross-section does not fulfil the requirements for all safety levels. For comparison, the resulting shear stress v_{Ed} is also compared to the average shear capacity $v_{R,c}$ (calculated assuming that the resistance factors equal one and using the average material properties). As can be seen from comparing Table 8 to Table 9, Level of Approximation II is less conservative than Level of Approximation I (average decrease of the Unity Check with 9.8 %) because it results in lower sectional shear forces, and thus follows the principles of a Level of Approximation approach (fib 2012).

Table 9: Shear capacity $v_{Rd,c}$, average shear capacity $v_{R,c}$, sectional shear v_{Ed}, and resulting unity checks UC. Conversion: 1 kN/m = 0.07 kip/ft, 1 MPa = 145 psi.

	Usage	Design
V_{Ed} (kN/m)	241	276
v_{Ed} (MPa)	0.477	0.547
$v_{Rd,c}$ (MPa)	0.538	0.538
UC	0.887	1.017
$v_{R,c}$	0.984	0.984
$v_{Ed}/v_{R,c}$	0.485	0.556

For both proof load locations, the punching capacity has been verified. At the shear-critical position, the Unity Check for punching is 0.95 and at the flexure-critical position UC = 0.93. A punching shear failure is thus not governing.

To have a better estimate of the average ultimate capacity of the slab that can be expected when loading until failure, the capacity is determined with the Extended Strip Model (Lantsoght et al. 2017d). The maximum expected load on the bending moment position is then 3297 kN (741 kip) and on the shear position 3025 kN (680 kip).

Lastly, the shear capacity of the sidewalk, which has stirrups, has been verified. It was observed that shear failure could occur in the sidewalk before it occurs in the solid slab, and therefore the behavior of the sidewalk was monitored during testing.

The analysis of the cross-sections under study for the calculated values for the proof loading for bending and shear showed that the capacity was only found to be sufficient for some safety levels (but not all required levels) prior to proof loading the viaduct. The proof load test is thus a suitable tool to show experimentally that the bridge fulfils the code requirements. Since high loads are applied, for which prior to the load testing Unity Checks larger than one are found, the interpretation of the measured responses during the proof load test becomes of the utmost importance.

2.6 **Sensor plan**

Prior to a proof load test, saying that loading to a certain load level is safe or unsafe, is related to the calculations that are made (as discussed in §2.5) without the additional knowledge that proof loading offers the assessing engineers. During testing, the observed behavior in terms of deformations, strains, cracks, etc. form the first basis for determining whether loads can be further increased or not. The preparatory calculations are used as background for the decisions to further increase the load or not. As the load is increased, the importance of the measurements and interpretation thereof increases.

For viaduct Zijlweg, the following responses were monitored: deflections of the deck, deflections of the cross-beams, crack width, strain, movement in the joint, and acoustic emissions. The force in the jacks was measured separately with load cells. As the pilot proof load test was used to gain more experience in the technique of proof load testing and because stop criteria (especially for shear) are not well-defined yet, an extensive sensor plan was used. In total 16 LVDTs (linear variable differential transformers), 6 laser distance finders, 15 acoustic emission

sensors, and 4 load cells were used. The acoustic emission measurements were carried out for research purposes (Yang and Hordijk 2015). An overview of the sensor plan is given in Fig. 17. The LVDTs that are not shown in this figure are the reference LVDT that is used outside the loaded span to check the strain resulting from the effects of temperature and humidity (see Fig. 18), the three LVDTs used to follow the width of existing cracks, and the four LVDTs used to monitor the expansion joint.

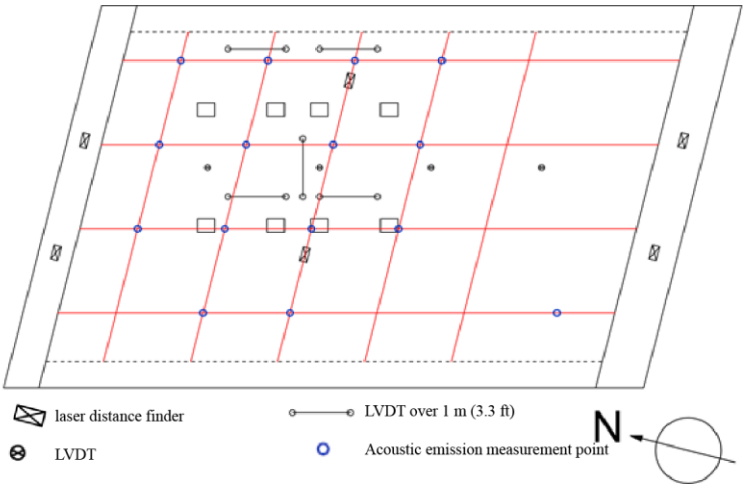

Fig. 17: Sensor plan of viaduct Zijlweg. Reprinted with permission from (Lantsoght et al. 2018a)

Fig. 18: Position of reference LVDT to measure influence of temperature and humidity. Picture showing support 5.

The lasers and LVDTs in the longitudinal direction at the middle of the notional lane are used to find the longitudinal deflection profile of the tested span. Two additional lasers are used at different positions in the transverse direction to find the transverse deflection profile. The deflections of the cross-beams are measured with two lasers per support. These measurements are used to measure the compression of the elastomeric bearings.

LVDTs are placed over existing cracks to monitor crack opening during the proof load test. On the side of the deck, a possible shear crack is monitored, and on the soffit of the crack, a longitudinal and transverse crack close to the center of the proof load tandem are monitored. To measure strains, LVDTs are placed over 1 m (3.3 ft) to find the average strain over this region. Two LVDTs are placed longitudinally and one LVDT is placed transversely to measure the longitudinal and transverse bending moments respectively. Finally, the movement in the joints is measured by using LVDTs of which one end is connected to the abutment and the other end to the slab. Two LVDTs are used to monitor the joint on the east side of the slab and two LVDTs on the west side.

3 EXECUTION OF PROOF LOAD TEST

3.1 **Loading protocol**

Two proof load tests were carried out: one proof load test at a flexure-critical position and one proof load test at a shear-critical position. Both tests were carried out in span 4, on June 17th 2015. The proper functioning of all sensors was verified during the afternoon of June 16th. A person jumping on the bridge resulted in small but measurable responses, see Fig. 19, and driving a car over the viaduct resulted in clear responses, see Fig. 20.

For the proof load tests at the shear- and flexure-critical positions, a setup with a load spreader beam, counterweights, and four hydraulic jacks was used. Fig. 21 shows a photograph of the load application system. Before the beginning of the proof load test, the jacks are not extended, and the load caused by the applied counterweight is carried off at the supports to the substructure. During the proof load test, the load on the jacks can be controlled and the superstructure (reinforced concrete slab) is loaded.

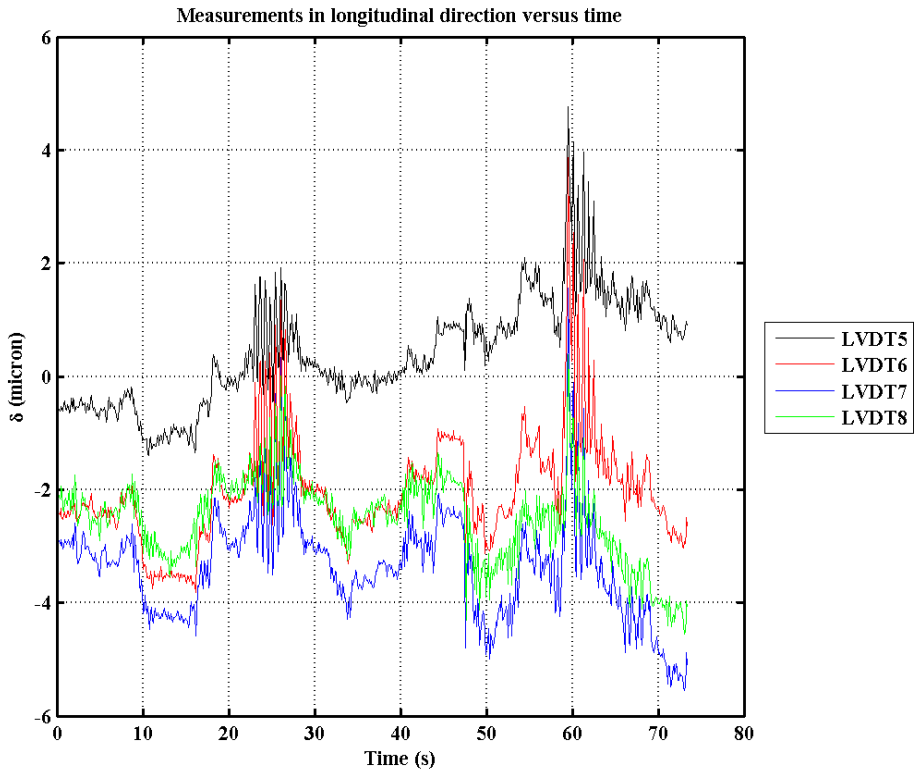

Fig. 19: Measurement of person jumping. Conversion: 1 micron = 4×10^{-5} in.

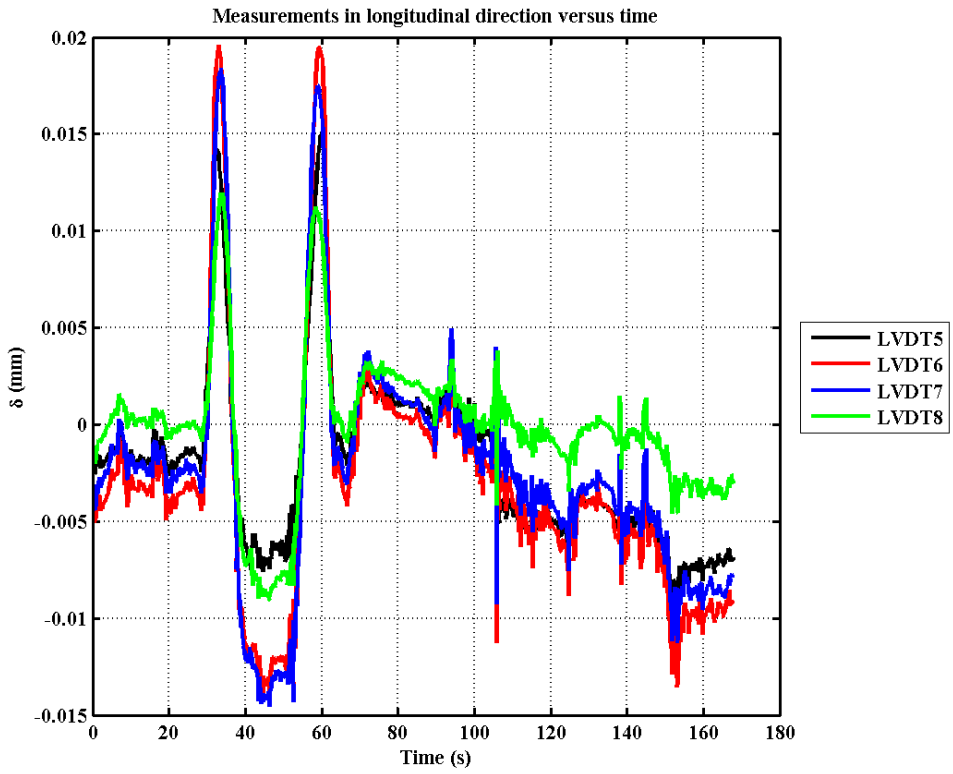

Fig. 20: Measurement of car passing. Conversion: 1 micron = 4×10^{-5} in.

Fig. 21: Setup of the load used on viaduct Zijlweg.

To measure the repeatability and linearity of the response, and to follow the acoustic emission measurements, a cyclic loading protocol was selected. This protocol also allowed for the verification of the stop criteria after each cycle of loading and unloading. The loading protocol used at the flexure-critical position is shown in Fig. 22a and the loading protocol used at the shear-critical position in Fig. 22b. The first level of 400 kN (90 kip) was used to check the responses of all sensors. The second load level corresponds to the serviceability limit state. The third and fourth load level are intermediate load levels. The final load level corresponds to a load slightly larger than the safety level RBK design. This load level was only applied once. A baseline load level of 100 kN (23 kip) is used between the load cycles to keep all jacks and sensors activated. The maximum load in the bending moment test was 1368 kN (308 kip) when the weight of the jacks and steel plate are taken into account. The maximum load in the shear test was 1377 kN (310 kip) when all loading is considered.

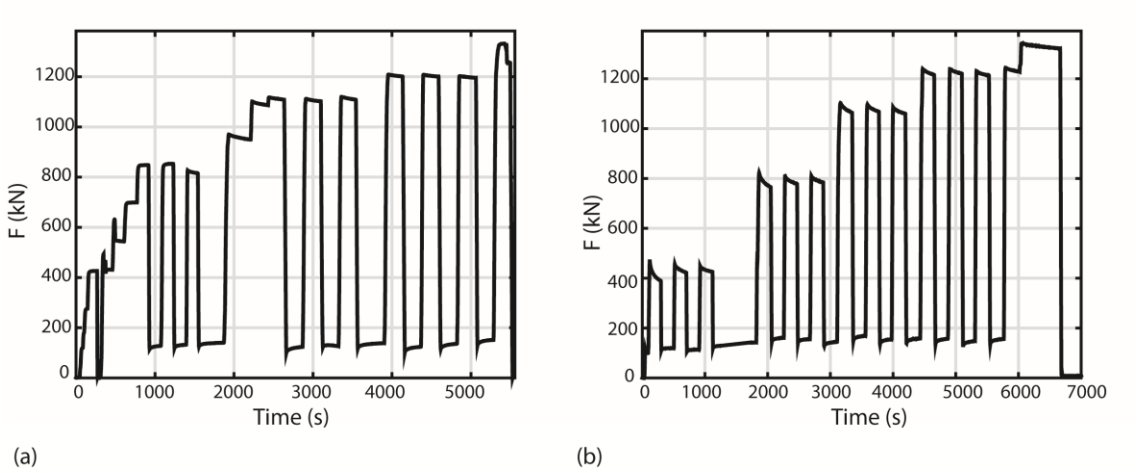

Fig. 22: Loading protocol: (a) bending moment test; (b) shear test. Conversion: 1 kN = 0.225 kip.

3.2 **Measurements and observations**

3.2.1 *Load-deflection curves*

The envelope of the load-displacement curve of the bending moment test is shown in Fig. 23. Some reduction of the stiffness can be observed for increasing loads, which may be caused by redistribution of stresses in the transverse direction. A reversal of the stiffness occurred during the unloading branch after the proof load test. The envelope of the load-deflection diagram for the shear-critical position is shown in Fig. 23. From this graph, it can be seen that during this proof load test, the behavior was fully linear. The observed stiffness in the test at a shear-critical position is larger than for the flexure-critical position, which was expected as a result of the loading position closer to the support for the shear-critical position.

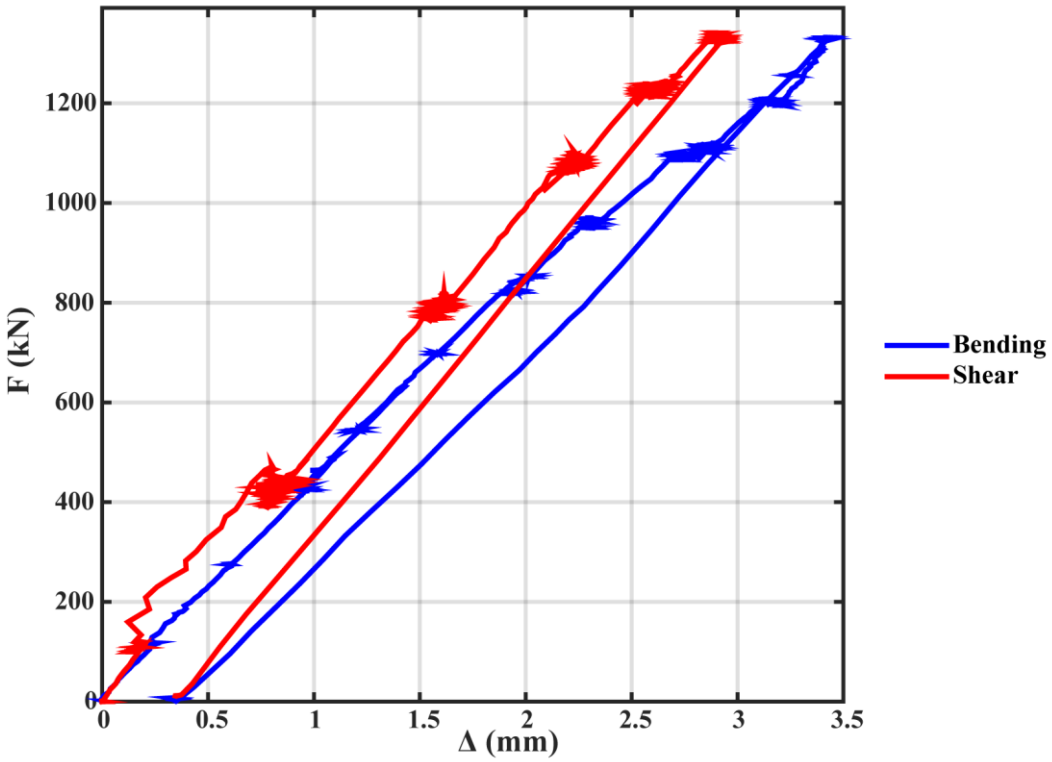

Fig. 23: Envelope of the force-displacement diagram for the flexure-critical and shear-critical position. Conversion: 1 kN = 0.225 kip, 1 mm = 0.04 in.

3.2.2 *Deflection profiles*

The longitudinal deflection profile obtained during the bending moment test is shown in Fig. 24a. From the longitudinal deflection profiles, it can be seen that no significant changes occur in the structural behavior. The transverse deflection profile is shown in Fig. 24b. A change in the behavior in the transverse direction can be seen. The stiffness of the sidewalk is not the same as the stiffness of the carriageway. At low load levels, the sidewalk deflects more because of the presence of cracks. At higher load levels, the stirrups are activated and the sidewalk behaves in a stiffer way than the carriageway.

The longitudinal deflection profile resulting from loading at a shear-critical is shown in Fig. 25a. At two intermediate load levels, the deflection profile is disturbed. An analysis of the data showed that for this range of loads, a shift in the values of the measuring LVDT occurred, possibly caused by the sensor being unable to be further compressed. The transverse deflection profile is fully linear, see Fig. 25b. The structural response under the sidewalk is stiffer than under the carriageway, caused by the different reinforcement layout.

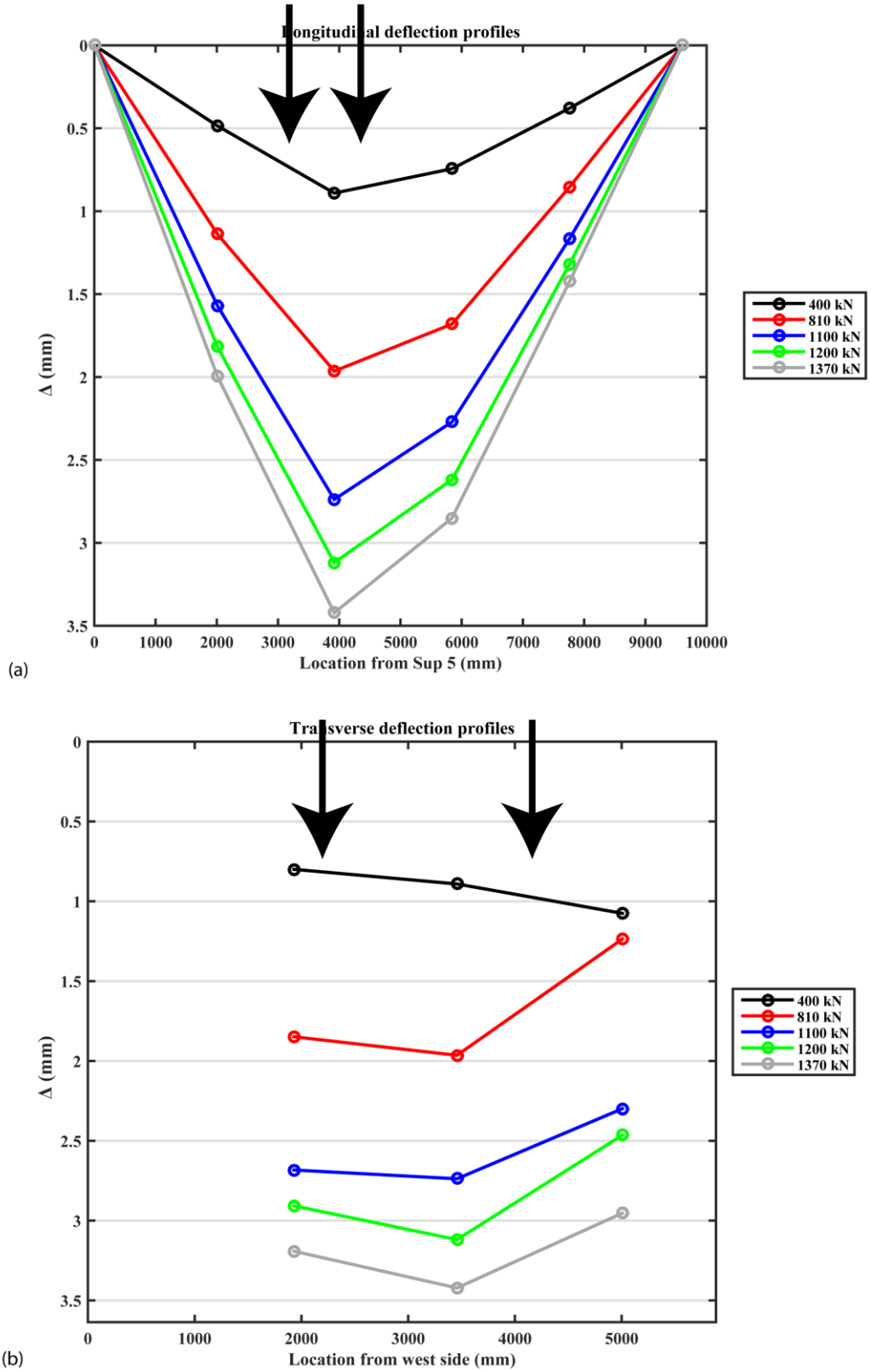

Fig. 24: Deflection profiles for loading at flexure-critical position: (a) longitudinal profile; (b) transverse profile. Arrows indicate position of centre of axles. Conversion: 1 kN = 0.225 kip, 1 mm = 0.04 in.

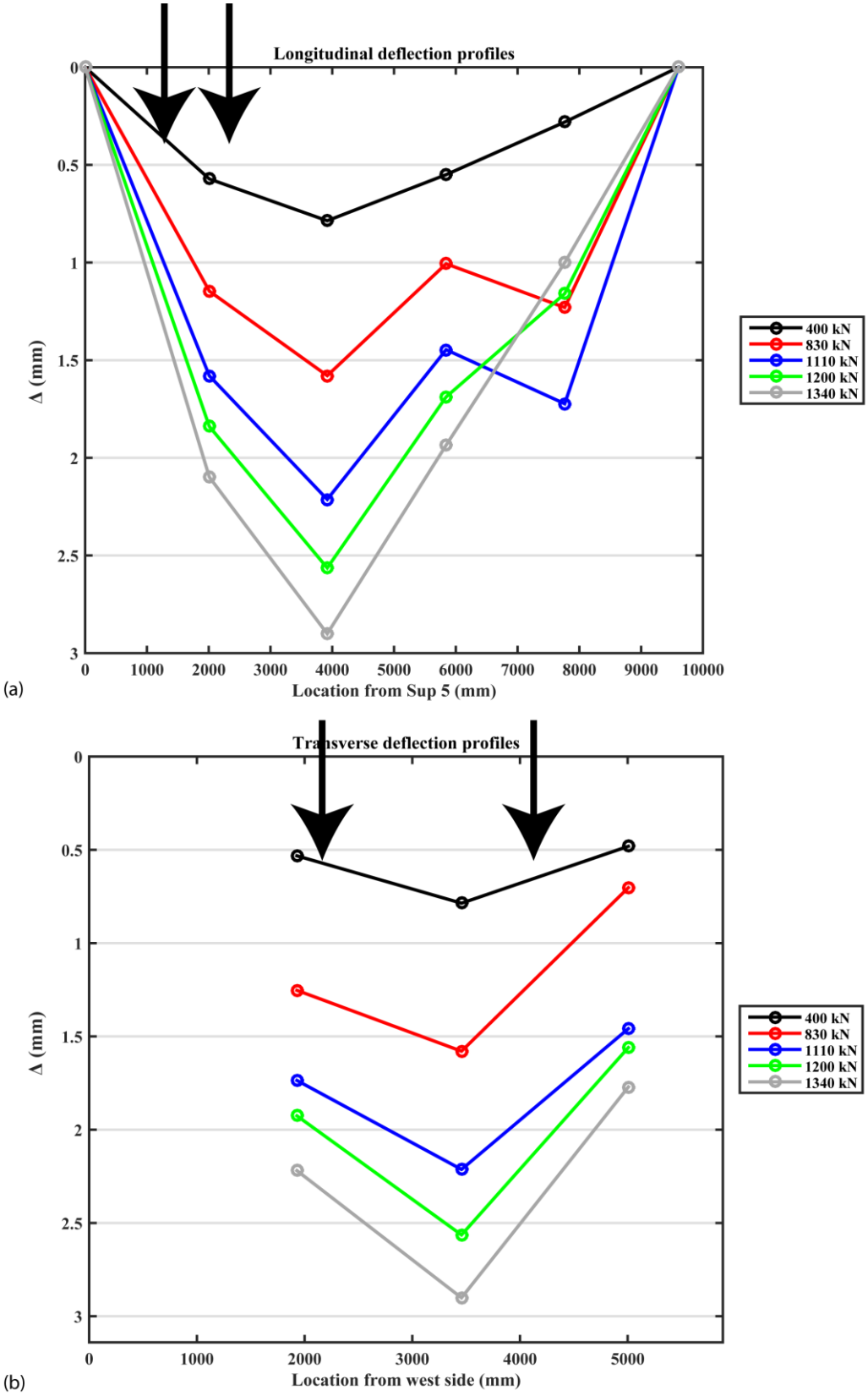

Fig. 25: Deflection profiles for loading at shear-critical position: (a) longitudinal profile; (b) transverse profile. Arrows indicate position of centre of axles. Conversion: 1 kN = 0.225 kip, 1 mm = 0.04 in.

3.2.3 *Strains and crack width*

For strains and the increase in crack width, LVDTs were placed horizontally on the slab soffit. During the bending moment test, the strains at the bottom were measured and a linear relation between the applied load and resulting strains was observed, see Fig. 26a. The increase in crack width for the applied load is shown in Fig. 27a. The largest increase in crack width is less than 0.04 mm (0.0016 in), so that the effect of cracking can be considered negligible, since cracks smaller than 0.05 mm (0.0020 in) are typically not considered as structural.

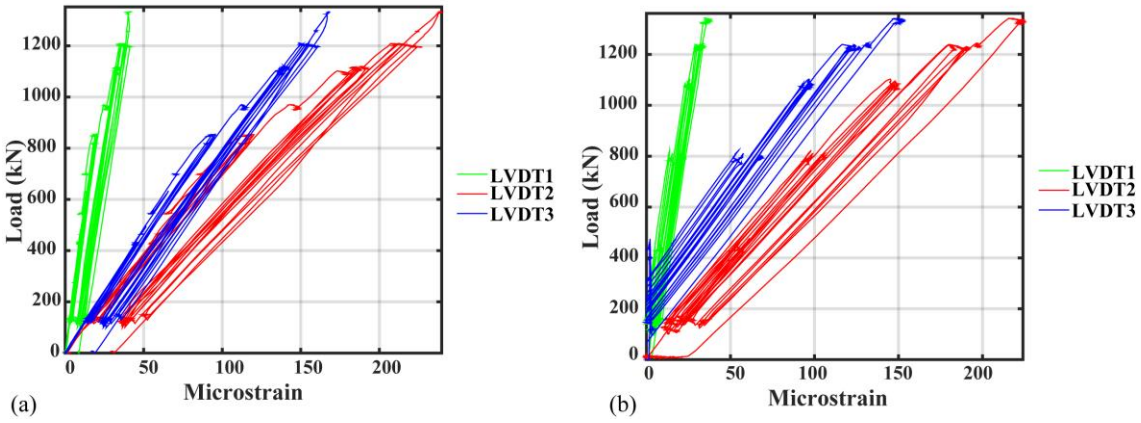

Fig. 26: Relation between strain and load: (a) during the bending moment proof load test; (b) during the shear test. Conversion: 1 kN = 0.225 kip.

For the shear test, no nonlinear behavior was observed from the measurements of the strains, see Fig. 26b. The increase in crack width for the applied load is shown in Fig. 27b. The largest increase in crack width is less than 0.025 mm (0.0010 in), so that the effect of cracking can be considered negligible.

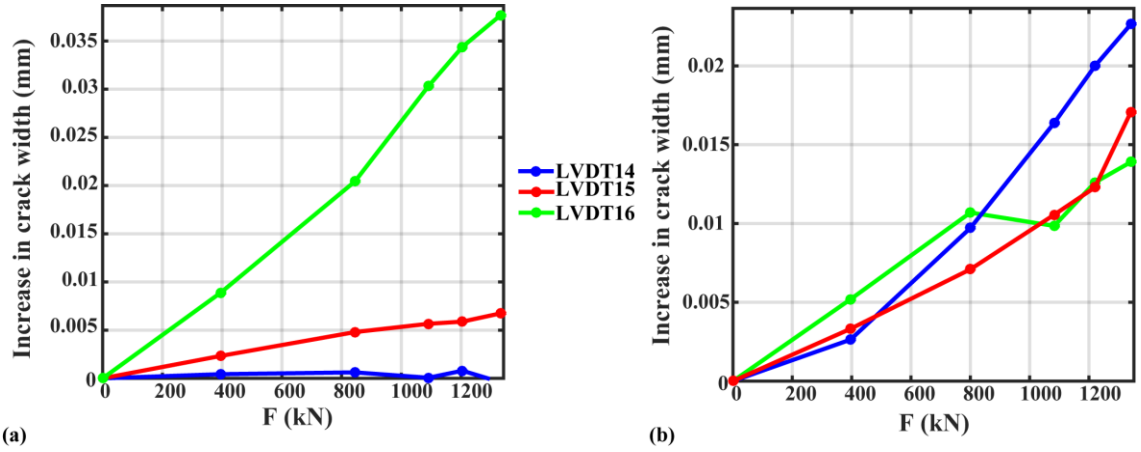

Fig. 27: Increase in crack width: (a) during the bending moment proof load test; (b) during the shear proof load test. Conversion: 1 mm = 0.04 in, 1 kN = 0.225 kip.

3.2.4 *Movement in joint*

The results of the measurements of the LVDTs applied over the expansion joint are given in Fig. 28. As the measurements are started at the beginning of the proof load test, it makes sense that a negative displacement is measured during the test. The test is carried out with a system of a steel spreader beam, jacks, and counterweights. Prior to the test, all load goes to the supports and affects the joint due to small eccentricities in the setup. During the test, the jacks apply the load to the superstructure, which results in unloading of the joint. The last part of the measurements (7000 s and further in Fig. 28) correspond to the removal of the counterweights (per ballast block), which results in unloading of the joint.

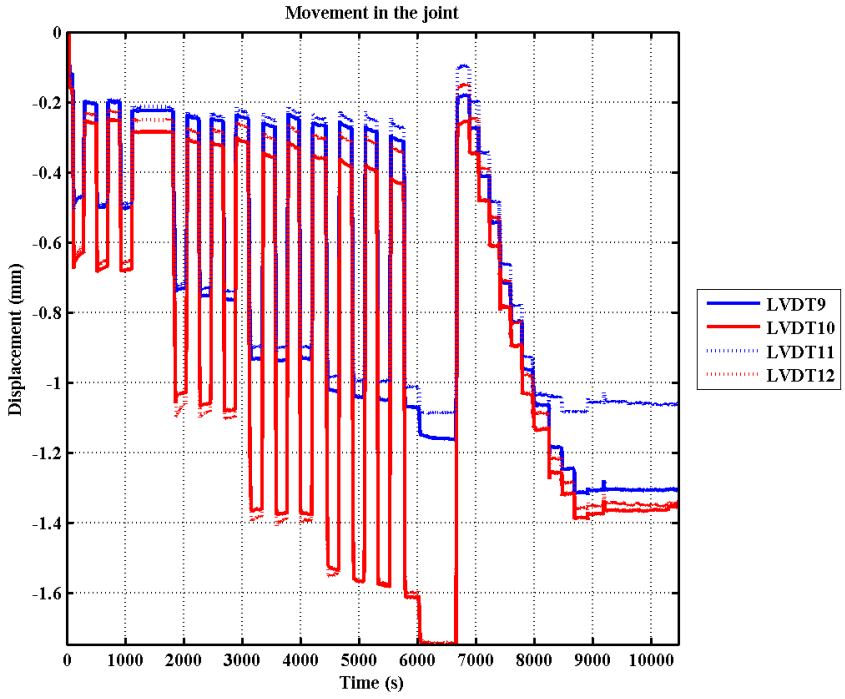

Fig. 28: Movement in the joint during the shear proof load and during removal of the counterweight. Conversion: 1 mm = 0.04 in.

3.2.5 *Influence of temperature*

The strains caused by changes in temperature and humidity are measured by the reference LVDT (see Fig. 18). The information of the ambient temperature can be taken from the Dutch meteorological institute (Royal Dutch Meteorological Institute 2017). The measurement of the temperature of the bridge deck is part of the monitoring system for ASR, as discussed in §2.3.3. During the bending moment test, see Fig. 29a, the bridge deck temperature and ambient temperature increased similarly. The measured strain is inversely proportional to the temperature. As

the temperature increases, the aluminum strip expands. This expansion leads to compression of the LVDT, or negative values.

For the shear proof load test, see Fig. 29b, the observations are different: the ambient temperature decreased but the temperature of the bridge deck increased slightly. The weather conditions explain this behavior: the wind was blowing, reducing the ambient temperature, and at the same time, the sun was shining, warming up the bridge deck. The measurements of the reference LVDT are in correspondence to the ambient temperature.

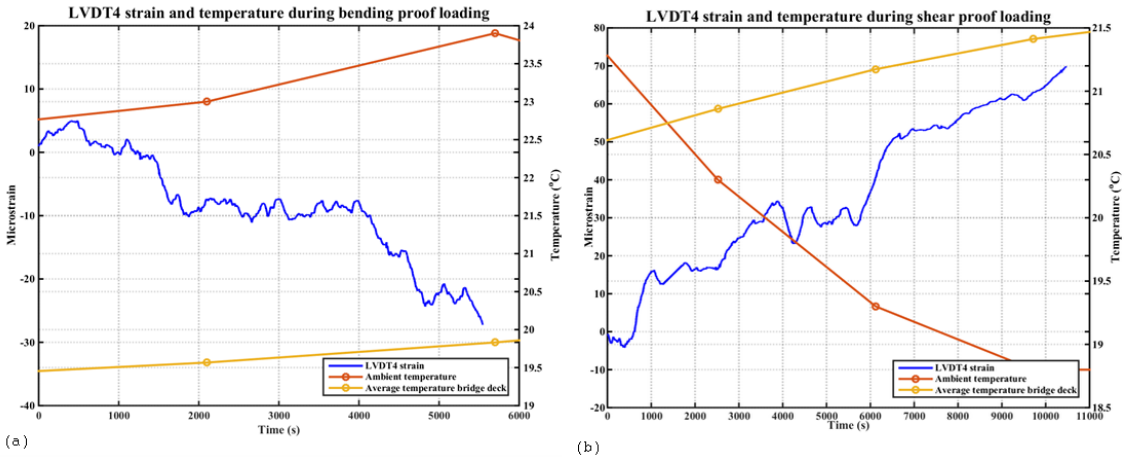

Fig. 29: Reference strain and temperature during: (a) testing at flexure-critical position; (b) testing at shear-critical position.

4 POST-PROCESSING AND RATING

4.1 **Development of final graphs**

After the proof load test, the final graphs are developed and reported. These graphs are similar to the graphs that are observed in real-time during the experiment in the field. The net deflections are found by subtracting the deflections of the supports from the deflections measured over the span. The net strains result from subtracting the reference strain for environmental effects from the measured strains in the tested span. The graphs shown in §3.2 are the post-processed graphs from testing viaduct Zijlweg.

4.2 **Comparison with stop criteria**

4.2.1 *ACI 437.2M acceptance criteria*

The limit of residual deformation to maximum deformation according to ACI 437.2M-13 (ACI Committee 437 2013) is 25%. In the bending moment test, the maximum deflection is Δ_{max} = 3.42 mm (0.14 in) and the residual deflection is Δ_{res} 0.333 mm (0.013 in), resulting in a ratio of 9.7%. The acceptance criterion is thus fulfilled. For the shear test, Δ_{max} = 2.9 mm (0.11 in) and Δ_{res} = 0.28 mm (0.01 in), so that the ratio equals 9.7%. The acceptance criterion is fulfilled.

The remaining acceptance criteria from ACI 437.2M-13 (ACI Committee 437 2013) are the permanency ratio and deviation from linearity index. These acceptance criteria are directly related to the cyclic loading protocol described by ACI 437.2M-13. As such, they cannot be evaluated for the different loading protocol that is used for testing viaduct Zijlweg.

4.2.2 *German guideline stop criteria*

The limit of residual deformation to maximum deformation according to the German guideline (Deutscher Ausschuss für Stahlbeton 2000) is 10%. As mentioned in §4.2.1, the maximum ratio in the bending moment test was 9.7%. The stop criterion for residual deflection was thus never exceeded. Similarly, for the shear test, the stop criterion for residual deflection was not exceeded during the proof load test.

The stop criterion for concrete strains is:

$$\varepsilon_c < \varepsilon_{c,lim} - \varepsilon_{c0} \tag{1}$$

with ε_c the measured strain, $\varepsilon_{c,lim}$ = 800 $\mu\varepsilon$ for concrete compressive strengths above 25 MPa (3.6 ksi), and ε_{c0} the strain caused by the permanent loads present at the time of the proof load test. The value of ε_{c0} can be taken from the output of the finite element program described in §2.4.1. The maximum strain measured during the bending moment experiment is 240 $\mu\varepsilon$ when corrected for the effect of temperature and humidity. The corresponding strain due to permanent loads at the positon where the maximum strain was measured is 38 $\mu\varepsilon$. The maximum strain in the experiment would thus be 762 $\mu\varepsilon$, which is not exceeded. The stop criterion is thus not exceeded. For the shear test, ε_c = 224 $\mu\varepsilon$ (corrected with the reference strain for environmental effects) and the strain due to permanent loads is ε_{c0} = 45 $\mu\varepsilon$. The limiting strain, 755 $\mu\varepsilon$ is not exceeded and the stop criterion is never exceeded during the experiment.

The limiting crack width and residual crack width form a stop criterion in the German guideline as well. However, since none of the crack widths measured are larger than 0.05 mm (0.002 in), no structural cracking occurs and this stop criterion is not exceeded.

4.2.3 *Proposed stop criteria*

The proposed stop criteria (Lantsoght et al. 2018b) are compared with the measurements on viaduct Zijlweg. The stop criteria are based on the concrete strain, the limiting crack width, the stiffness, the load-deflection diagram, the longitudinal deflection profiles and the transverse deflection profiles.

The stop criteria related to the load-deflection diagram, and longitudinal and transverse deflection profiles are qualitative in nature. As shown in §3.2.1 and §3.2.2, no signs of nonlinear behavior were observed from these plots. The limiting crack width only needs to be verified for crack widths larger than 0.05 mm (0.0020 in). The data in §3.2.3 show that none of the cracks that were monitored during the proof load tests were activated.

The stop criterion for the limiting concrete strain ε_{stop} is for flexure:

$$\varepsilon_c < \varepsilon_{stop} \tag{2}$$

with ε_c the measured strain, and:

$$\varepsilon_{stop} = 0.65\varepsilon_{bot,\max} - \varepsilon_{c0} \tag{3}$$

$$\varepsilon_{bot,\max} = \frac{h-c}{d-c} 0.9 \frac{f_y}{E_s} \tag{4}$$

with ε_{c0} the strain caused by permanent loads, h the height of the member, d the effective depth of the member, c the height of the compression zone when the strain in the steel is 90% of the yield strain, f_y the yield stress of the steel, and E_s the Young's modulus of the steel. The limiting strain ε_{stop} for the flexure-critical position is 751 $\mu\varepsilon$. This value is never exceeded, as can be seen in Fig. 26a. Until a suitable stop criterion is developed based on research, the stop criterion for the limiting concrete strain for shear is kept as the same criterion used in the German guideline, Eq. (1), which was not exceeded during the proof load test for shear.

For flexure and shear, the stiffness (measured as the tangent to the load-displacement diagram) during the proof load test cannot be less than 75% of the initial stiffness. In other words, the maximum reduction of the stiffness that is allowed is 25%. In the bending moment test, the

stiffness reduction was 4%. In the shear test, the stiffness reduction was 12%. The stop criterion for the stiffness is thus never exceeded.

As shown in the previous paragraphs, none of the proposed stop criteria were exceeded during the proof load tests for flexure and shear. This observation corresponds with the conclusions that were drawn from the extensive sensor plan on the viaduct: no nonlinear behavior or signs that irreversible damage had occurred were observed during the proof load test. The bridge could thus withstand the applied target proof load, representative of the factored live loads. Therefore, it was shown experimentally that the tested element of the bridge (the superstructure) fulfils the requirements of the code.

4.3 **Final rating**

The proof load tests on the viaduct Zijlweg were successful. The planning and preparation facilitated the execution of the test. All sensors and the data acquisition system functioned properly and allowed for an evaluation of the data in real time. The goal of the proof load test, i.e. to show that the superstructure fulfils the code requirements, was also met based on the current knowledge on proof load testing. Further research is necessary to confirm assumptions made in the procedures. The highest safety level that was fulfilled (according to current knowledge) is the RBK Design level (with 5% extra loading). During the proof load experiment, there was no sign of distress in the measurements. If the currently followed procedures can be confirmed with further research, the field tests have shown that it is safe to keep the viaduct open to all traffic. Until then, however, it has been shown that the bridge is not unsafe, but it is not necessarily demonstrated that the bridge is safe. The result of the proof load test is important, because the uniaxial tensile strength of the concrete in the viaduct is measured to be very low as a result of damage caused by alkali-silica reaction, so that the shear capacity of this viaduct was subject to discussion. The results of the proof loading test and the past experiments in the laboratory (see §2.3.1) indicate that, even though it is not possible to quantify the reduction or increase in the capacity of an element with ASR-damage, the problems for existing bridges appear to be limited. When a proof load test demonstrates sufficient capacity for an existing bridge, the cost of replacement of the superstructure is avoided (Lantsoght 2017). This cost includes the direct economic cost, but also the environmental cost associated with the CO_2 emissions of the materials and transportation of materials, and the social cost of driver delays.

4.4 Lessons learned and recommendations for practice

Based on the experience of the proof load test on the viaduct Zijlweg, the following lessons learned can be identified:

- Proof load testing for shear is possible and gives valuable results.
- The presented case study is a good example of a bridge with large uncertainties on the capacity caused by ASR cracking. It shows that load testing can be used for the assessment of existing bridges when the uncertainties on the capacity are large. The conclusion is that for such cases proof load testing is an interesting and economic method.

The following practical recommendations result from the pilot proof load test:

- A good preparation for the proof load test is essential.
- It is necessary to carry out a visual inspection, so that the limitations on site can be identified during the preparation stage. For the case of viaduct Zijlweg in particular, marking positions on the top face of the bridge was made difficult because of the sidewalk.
- Selecting the critical crack that should be monitored during a proof load test is difficult. Either the test engineers should follow the crack width of a number of cracks during the test, or non-contact methods should be used to follow all cracks within a certain region.
- The presented loading method with the steel spreader beam and counterweights performs well in practice and can be recommended for proof load testing.
- For shear-critical bridges and bridges with large uncertainties, an extensive preparation and a large number of sensors during the test are necessary to avoid a brittle failure during the test. For other bridge types, a shorter and simpler approach to proof load testing should be developed, so that with minimal preparation and equipment an answer can be found to the question of whether the bridge fulfils the code requirements or not.
- To save time in the field, non-contact sensors should be applied where feasible. The use of non-contact sensors, and stop criteria related to the output of such sensors, requires further research and pilot testing.

4.5 **Discussion and elements for future research**

Proof load testing of shear-critical reinforced concrete slab bridges requires a thorough understanding of shear-critical concrete structures and currently a large number of uncertainties on this method still exist. As such, it is not possible yet to develop a step-by-step method for proof load testing of shear-critical concrete bridges that can be implemented in a code or guideline. The main uncertainties at this moment are the definition of safe stop criteria for shear-critical concrete bridges and the determination of the target proof load. To develop safe stop criteria for reinforced concrete slab bridges, further experimental work is necessary to study crack development in laboratory conditions. If safe stop criteria are available, it also becomes possible to load a bridge past the target proof load and until reaching the first stop criterion, to learn about the full linear elastic range of the bridge and to know the maximum live load on the bridge. To verify the currently used simple approach for determining the target proof load, a probabilistic study is necessary so that the target proof load indeed represents the required reliability index for the tested bridge.

A limitation of a proof load test with only two loading positions is that in fact only the experimental results from two positions are obtained. To extrapolate this result to all positions of the bridge, which may have some local weaknesses perhaps, is an element that need further probabilistic studies. Currently, an additional few % of load is applied to cover variability and uncertainties on the method itself, but this number should be quantified with rigorous studies.

A proof load test does not result in the experimental capacity of a tested bridge as this would require a test to failure. However, it gives a lower bound of the capacity and can express the capacity in terms of traffic that the bridge can carry.

5 SUMMARY AND CONCLUSIONS

On June 17th 2015, a proof load test was carried out on the viaduct Zijlweg in the province of Noord Brabant, the Netherlands. Two positions were identified for testing: a flexure-critical position and a shear-critical position. The viaduct Zijlweg was selected for proof loading, as it showed severe cracking caused by alkali-silica reaction (ASR) damage. Therefore, the capacity of the viaduct, especially its shear capacity, was subject to discussion. To evaluate the effect of ASR, monitoring of the expansion, temperature, and moisture was installed in 2003. The end span was tested, as this span is not directly located above the highway.

The literature review on ASR and the behaviour of structural elements with ASR-damage showed that the uniaxial tensile strength of concrete with ASR-damage is very low. The effect of ASR on the shear capacity is subject to discussion. For small elements, no reduction, or even an increase in the shear capacity of an ASR-damaged beam as compared to an undamaged beam was observed. These beams were fabricated in the laboratory and subjected to higher temperatures and moisture cycles to activate the swelling of the ASR-gel. For beams sawn from a viaduct with ASR-damage the shear capacity was 75% of the theoretically predicted capacity. In some experiments, an increase in the capacity was found for the ASR-affected elements. This increase was attributed to the prestressing induced in the sections by the restraint of the swelling. Load testing on ASR-deteriorated bridges in Japan, France, South Africa, and Denmark in the past did not result in a marked influence of the ASR-damage on the measured response of the structures.

The position and magnitude of the target proof load were determined by using a linear elastic finite element model. For the bending moment proof load test, the position of the proof loading tandem was determined by finding the most unfavourable position of the design truck in the finite element model. The live loads were then replaced by the proof load tandem at the critical position. The magnitude of the load on the proof load tandem was then increased until it reaches the bending moment that was found by using the load combination from the code. This procedure is followed for the different safety levels, which each use a different set of safety factors. For the shear proof load test, the critical position is at 2.5d. The target proof load to get the same sectional shear as for the load combination from the code was then determined. Further probabilistic studies are required to develop a better method for determining the target proof load. An assessment prior to the test showed that at the RBK Design Level, the viaduct does not fulfil the requirements for shear and bending.

The viaduct was heavily instrumented during both load tests to carefully monitor the structural behaviour. Currently, no suitable and safe stop criteria for shear-critical reinforced concrete slab bridges exist. The large amount of sensors applied served the purpose of catching signs of possible nonlinearity or occurrence of irreversible damage, as stop criteria (especially for shear) are still a subject of research. A cyclic loading protocol was used for the analysis. The maximum load in the bending moment test corresponds with the safety level RBK Design + 9%. The maximum load in the shear test corresponds with the safety level RBK Design + 12%.

The proof load test was carried out at a flexure-critical and at a shear-critical position. For both proof load tests, it was found that the viaduct could carry loads corresponding to the safety level RBK Design (and some extra reserve) without signs of distress. Given the uncertainties on

the method and need for future research, the final conclusion about the viaduct is that it has been shown that the viaduct is not unsafe, but it has not yet been shown that it is safe and that it fulfils the code requirements. Regular inspections and analysis of the ASR data is necessary, as the remaining space in the expansion joints is small. The proof load test on the viaduct in the Zijlweg showed the important conclusion that the capacity of a viaduct affected by ASR is higher the analytically determined capacity, since the Unity Check for the applied load was analytically determined to be larger than 1. The problem of the small strength of the concrete in uniaxial tension is thus of a lower magnitude than feared.

REFERENCES

ACI COMMITTEE 437 2013. Code Requirements for Load Testing of Existing Concrete Structures (ACI 437.2M-13) and Commentary Farmington Hills, MA.

AHMED, T., BURLEY, E. & RIGDEN, S. 1998. The static and fatigue strength of reinforced concrete beams affected by alkali-silica reaction. *ACI Materials Journal,* 95**,** 376-388.

AHMED, T., BURLEY, E. & RIGDEN, S. 1999. Effect of alkali-silica reaction on tensile bond strength of reinforcement in concrete tested under static and fatigue loading. *ACI Materials Journal,* 96**,** 419-428.

BORSJE, H., PEELEN, W. H. A., POSTEMA, F. J. & BAKKER, J. D. 2002. Monitoring Alkali-Silica Reaction in Structures. *Heron,* 47**,** 96-109.

CEN 2002. Eurocode – Basis of structural design, NEN-EN 1990:2002 Brussels, Belgium: Comité Européen de Normalisation.

CEN 2003. Eurocode 1: Actions on structures - Part 2: Traffic loads on bridges, NEN-EN 1991-2:2003. Brussels, Belgium: Comité Européen de Normalisation.

CEN 2005. Eurocode 2: Design of Concrete Structures - Part 1-1 General Rules and Rules for Buildings. NEN-EN 1992-1-1:2005. Brussels, Belgium: Comité Européen de Normalisation.

CODE COMMITTEE 351001 1995. *NEN 6720 Technical Foundations for Building Codes, Concrete provisions TGB 1990 - Structural requirements and calculation methods (VBC 1995),* Delft, The Netherlands, Civil engineering center for research and regulation, Dutch Normalization Institute,.

CODE COMMITTEE 351001 2011. *Assessement of structural safety of an existing structure at repair or unfit for use - Basic Requirements, NEN 8700:2011 (in Dutch),* Delft, The Netherlands, Civil center for the execution of research and standard, Dutch Normalisation Institute.

COPE, R. J. 1985. Flexural Shear Failure of Reinforced-Concrete Slab Bridges. *Proceedings of the Institution of Civil Engineers Part 2-Research and Theory,* 79**,** 559-583.

DEN UIJL, J. A. & KAPTIJN, N. 2002. Structural consequences of ASR: an example on shear capacity. *Heron,* 47**,** 1-13.

DEUTSCHER AUSSCHUSS FÜR STAHLBETON 2000. DAfStb-Guideline: Load tests on concrete structures (in German). Deutscher Ausschuss fur Stahlbeton,.

FIB 2012. *Model code 2010: final draft,* Lausanne, International Federation for Structural Concrete.

GIACCIO, G., ZERBINO, R., PONCE, J. M. & BATIC, O. R. 2008. Mechanical behavior of concretes damaged by alkali-silica reaction. *Cement and Concrete Research,* 38**,** 993-1004.

HADDAD, R. H., SHANNAG, M. J. & AL-HAMBOUTH, M. T. 2008. Repair of reinforced concrete beams damaged by alkali-silica reaction. *Aci Structural Journal,* 105**,** 145-153.

KOENDERS INSTRUMENTS 2015. Zijlweg monitoring systeem.

LANTSOGHT, E. O. L. 2017. Chapter 9: Field assessment of a concrete bridge. *In:* PACHECO-TORGAL, F., MELCHERS, R., SHI, X., SAEZ, A., DE BELIE, N. & VAN TITTELBOOM, K. (eds.) *Eco-efficient Repair and Rehabilitation of Concrete Infrastructures.* Cambridge, UK: Woodhead Publishing.

LANTSOGHT, E. O. L., DE BOER, A. & VAN DER VEEN, C. 2017a. Distribution of peak shear stress in finite element models of reinforced concrete slabs. *Engineering Structures,* 148**,** 571-583.

LANTSOGHT, E. O. L., DE BOER, A. & VAN DER VEEN , C. 2017b. Levels of Approximation for the shear assessment of reinforced concrete slab bridges. *Structural Concrete,* 18**,** 143-152.

LANTSOGHT, E. O. L., KOEKKOEK, R. T., HORDIJK, D. A. & DE BOER, A. 2017c. Towards standardization of proof load testing: pilot test on viaduct Zijlweg. *Structure and Infrastructure Engineering***,** 16.

LANTSOGHT, E. O. L., VAN DER VEEN, C., DE BOER, A. & ALEXANDER, S. D. B. 2017d. Extended Strip Model for Slabs under Concentrated Loads. *ACI Structural Journal,* 114**,** 565-574.

LANTSOGHT, E. O. L., VAN DER VEEN , C., DE BOER, A. & HORDIJK, D. A. 2017e. Proof load testing of reinforced concrete slab bridges in the Netherlands. *Structural Concrete,* 18**,** 597-606.

LANTSOGHT, E. O. L., VAN DER VEEN , C., DE BOER, A. & HORDIJK, D. A. 2018a. Assessment of slab bridges through proof loading in the Netherlands. *ACI SP 323 Evaluation of Concrete Bridge Behavior through Load Testing – International Perspectives*.

LANTSOGHT, E. O. L., VAN DER VEEN, C., DE BOER, A. & WALRAVEN, J. C. 2013. Recommendations for the Shear Assessment of Reinforced Concrete Slab Bridges from Experiments *Structural Engineering International,* 23**,** 418-426.

LANTSOGHT, E. O. L., VAN DER VEEN , C. & HORDIJK, D. A. 2018b. Proposed stop criteria for proof load testing of concrete bridges and verification. *IALCCE 2018.* Ghent, Belgium.

LI, Y., VROUWENVELDER, T., WIJNANTS, G. H. & WALRAVEN, J. 2004. Spatial variability of concrete deterioration and repair strategies. *Structural Concrete,* 5**,** 121-129.

NEDERLANDS NORMALISATIE INSTITUUT 1963. Voorschriften voor het ontwerpen van stalen bruggen

NEVILLE, A. 2012. *Properties of Concrete, 5th edition,* Pearson Education

NIJLAND, T. G. & SIEMES, A. J. M. 2002. Alkali-Silica Reaction in The Netherlands: Experiences and current research. *Heron,* 47**,** 81-84.

NORMCOMMISSIE 351001 2011a. *Assessement of structural safety of an existing structure at repair or unfit for use - Basic Requirements, NEN 8700:2011 (in Dutch),* Delft, The

Netherlands, Civil center for the execution of research and standard, Dutch Normalisation Institute.

NORMCOMMISSIE 351001 2011b. Eurocode 1 - Actions on structures - Part 2: Traffic loads on bridges, EN 1991-2/NA:2011. Delft, The Netherlands: Civil engineering center for research and regulation, Dutch Normalization Institute.

PROJECTTEAM RWS/TNO BOUW 1997a. Safety evaluation existing structures: Reinforced concrete bridges (in Dutch).

PROJECTTEAM RWS/TNO BOUW 1997b. Veiligheidsbeoordeling voor bestaande constructies; Gewapend betonnen kunstwerken.

RAFLA, K. 1971. Empirische Formeln zur Berechnung der Schubtragfahigkeit von Stahlbetonbalken. *Strasse Brucke Tunnel,* 23**,** 311-320.

RIJKSWATERSTAAT 2002. Beheer- & Onderhoudsplan Viaduct Zijlweg gelegen over Rijksweg A59.

RIJKSWATERSTAAT 2008. Inspectierapport Programmernisinspectie Complex-cide 44G-113-01.

RIJKSWATERSTAAT 2013. Guidelines Assessment Bridges - assessment of structural safety of an existing bridge at reconstruction, usage and disapproval (in Dutch), RTD 1006:2013 1.1.

ROYAL DUTCH METEOROLOGICAL INSTITUTE. 2017. *Hourly weather data for the Netherlands* [Online]. Available: http://www.knmi.nl/klimatologie/uurgegevens/datafiles/350/uurgeg_350_2011-2020.zip. [Accessed 07/06/2017].

SCHMIDT, J. W., HANSEN, S. G., BARBOSA, R. A. & HENRIKSEN, A. 2014. Novel shear capacity testing of ASR damaged full scale concrete bridge. *Engineering Structures,* 79**,** 365-374.

SIEMES, T., HAN, N. & VISSER, J. 2002. Unexpectedly low tensile strength in concrete structures. *Heron,* 47**,** 111-124.

STEENBERGEN, R. D. J. M. & VROUWENVELDER, A. C. W. M. 2010. Safety philosophy for existing structures and partial factors for traffic loads on bridges. *Heron,* 55**,** 123-140.

TALLEY, K. G. 2009. *Assessment and Strengthening of ASR and DEF Affected Concrete Bridge Columns.* Ph.D. Thesis, The University of Texas at Austin.

TNO DIANA 2012. Users Manual of DIANA, Release 9.4.4. Delft, The Netherlands.

VERGOOSSEN, R., NAAKTGEBOREN, M., 'T HART, M., DE BOER, A. & VAN VUGT, E. 2013. Quick Scan on Shear in Existing Slab Type Viaducts. *International IABSE Conference, Assessment, Upgrading and Refurbishment of Infrastructures.* Rotterdam, The Netherlands.

WALRAVEN, J. C. 2010. Residual shear bearing capacity of existing bridges. *fib Bulletin 57, Shear and punching shear in RC and FRC elements; Proceedings of a workshop held on 15-16 October 2010.* Salò, Lake Garda, Italy.

WALRAVEN, J. C. 2012. Proof loading of concrete bridges (in Dutch). Stevin Report 25.5-12-9. Delft: Delft University of Technology.

WALRAVEN, J. C. 2013. Minimum shear capacity of reinforced concrete slabs without shear reinforcement: the value v_{min}. Stevin Report 25.5-12-4. Delft: Delft University of Technology.

WITTEVEEN+BOS 2014. Materiaalonderzoek Bruggen, zaaknummer 31084913: 44G-113-01 - Ongelijkvloerse kruising rijksweg - Zijlweg (Zijlweg). Deventer.

YANG, Y., DEN UIJL, J. A., DIETEREN, G. & DE BOER, A. 2010. Shear capacity of 50 years old reinforced cocnrete bridge deck without shear reinforcement. *3rd fib International Congress.* Washington DC, USA: fib.

YANG, Y. & HORDIJK, D. A. 2015. Acoustic Emission Measurement and Analysis on Zijlwegbrug. Stevin Report 25.5-15-01, Delft, The Netherlands: Delft University of Technology.